Establishing Viability of a Novel Wire Induction Extrusion 3D Printing Method

by

Michael James Knotts

A thesis submitted to the Graduate Faculty of
Auburn University
in partial fulfillment of the
requirements for the Degree of
Master of Science

Auburn, Alabama
August 8, 2020

Keywords: metal additive, additive manufacturing, casting, induction, aluminum

Approved by

Dr. Michael E. Zabala, Chair, Assitant Professor of Mechanical Engineering
Dr. Jordan Roberts, Lecturer, Mechanical Engineering
Dr. Dan Marghitu, Professor of Mechanical Engineering

Abstract

Metal additive manufacturing is an emerging area of fabrication for uses in research, industrial, and private fields. Currently, most of the common systems available for metal additive manufacturing have high costs associated with both acquisition and operation. In addition, they have several disadvantages including long build times, the need for highly controlled environments, and health risks associated with the powder used in many of the systems. This creates a need for development of alternative technologies capable of producing parts similar to other systems without these disadvantages.

Wire based systems avoid or decrease many of these disadvantages. They are low-cost, easy to operate, offer higher build speeds, and generally have fewer risks associated with them. However, wire can still be costly depending on the method, and does not have the same level of resolution that powder based systems have. By utilizing induction heating, high temperatures can be reached rapidly. Further, exploring the processes of molten and semi-solid extrusion allow for experimentation to achieve a system capable of precision performance while eliminating many disadvantages.

Developing a machine to utilize the advantages of wire-based printing in novel ways could allow for a low-cost alternative to current metal additive manufacturing methods. By integrating wire-feed, induction heating, a modular print head, and specialized designs for the bed and extrusion systems, this machine could fill the need for a competitive metal 3D printing technology at the fraction of the cost.

Tests to determine material properties for the parts produced by this method were conducted. This included hardness and tensile tests to find base characteristics regarding these

parts. The goal is to show with these tests that this is a competitive alternative to many current metal additive practices.

Acknowledgements

This research would not have been possible to complete without the aid of many individuals. I am deeply grateful for the contribution of everyone involved in helping me to achieve this, and cannot adequately express my thanks for the aid they provided.

Firstly, I would like to thank my family for the support they have shown me throughout my Master's program. They have been a constant source of encouragement during my studies and have helped in every way they were able. I know I would not be where I am without all they have done for me. For all of this I would like to say thank you to my parents, sister and her husband, and extended family.

I would like to also thank my committee for the guidance and help they have provided me. I am extremely thankful to Dr. Zabala for taking me on as a Master's student and helping me get my thesis on track to completion. I am also thankful to Dr. Roberts for his aid in design and testing issues and his encouragement, and to Dr. Marghitu for his feedback on data collection and research. Each member of my committee has been invaluable to the process.

There are several individuals who generously donated their time and energy to helping me in the development and testing of this technology as well. Travis Thompson and Jack Hudon were constant in their support and easing the workload, as well as assisting with the operation of the machine. They were a tremendous blessing throughout the entire project and I am thankful for all they have done. Dr. Wesley Hunko provided early guidance and design advice while simultaneously working on his own dissertation, and was a great help in getting started. Zane Oligee helped with programming a feed system as I had little experience in this area and was able to help us in making this area of the printer consistent. Greyson Harvill offered his expertise

with materials engineering to help in testing and evaluating samples produced by this method. This was beneficial in providing meaningful results on the success of the machine. In addition, all of the current DML/MTL TA's, both undergraduate and graduate, assisted me when I needed help with various tasks and eased the process along.

Lastly and most importantly, I would like to thank God for His constant blessings during this time and for providing me with the strength and endurance to see this to completion. Without His constant presence I would not have been able to continue during some of the great challenges I faced with this research.

Table of Contents

List of Tables

List of Figures:

Figure 25: Illustration of Rice's Semi-Solid Freeform Fabrication Setup.....36

Figure 26: Microstructure of Rice's Test Parts.....37

Figure 27: a) SSMED process graph, b) Single layer depositioning by the process.....39

Figure 28: Example of a Standard Tension Test Specimen.....40

Figure 29: Rockwell Hardness Test Method (Schematic Diagram).....41

Figure 30: Block Diagram of Printer Prototype.....39

I. Introduction

With the currently available methods of additive manufacturing being costly and oftentimes slow, there is a need for alternative methods to help the technology become more mainstream in its usage. This presents a real need for research and development into alternative and novel ways to produce parts via additive manufacturing. This research seeks to design, test, and validate a novel method.

Induction heating can be employed in the design and implementation of a novel approach to additive manufacturing. Induction heating uses electromagnetic fields created by alternating current traveling through a coil to heat electrically conductive material inside it. Using induction, an extrusion based method of additive manufacturing was developed. This method offers a tremendous decrease in cost to other methods currently available due to it's utilization of off the shelf materials, readily available feed stock, and design methods aiming to reduce complexity and expense.

To test this method, trial prints were produced to compare the geometrical accuracy of the prints. This was done by evaluating the percent error between the desired print and the measurements of the actual print. From here, layered samples were produced and prepared for materials testing. Rockwell hardness tests were performed on theses samples to help evaluate material properties of this method.

The initial results from this method appear promising. This method appears to be able to produce consistent prints close to the desired specifications. Further research is needed into more materials data and parameterization of this machine to fully verify the capabilities.

II: Scope and Objectives

The goal of this research was to design a new method of affordable and innovative metal additive manufacturing, as well as to conduct initial testing and validation of this method. The design stage entailed design of the print head, feed system, print bed, controls and motion of the machine. Each of these categories is a subsystem that has its own design concerns to be addressed.

After the design phase, strategies for producing samples are needed. The samples and methods from procuring them will be recorded for analysis. This will allow a preliminary evaluation of the performance of this machine and method. The samples will be measured based on the difference between desired dimensions and actual dimensions, as well as the hardness of layered samples.

The goal of these tests was to prove that this method is capable of producing repeatable results that match the desired part. While this testing only provides a baseline of operating conditions and results, the information provided from these is crucial to further development and examination of this technology. It is likely that, while the machine displays results that indicate it is capable of producing reliable parts, further testing and redesign would be needed to take it further.

III. Literature Review

Metal Additive Manufacturing:

Metal additive manufacturing is the process of fabricating a part by depositing material in a desired pattern as opposed to removing material from stock. There are currently two major categories for metal additive manufacturing, designated by the type of feedstock that is used. These are powder systems and wire systems. Powder systems can be further broken down into powder bed and powder fed systems. [1] While powder bed systems are typically the most commonly used machines in industry, processes and methods of the three machines provide different advantages and drawbacks, and different applications may seek to employ a different method.

Wong, et al, provided an alternate breakdown of additive manufacturing processes based on the state of the material in use. "[T]he criterion used is to classify these processes into liquid base, solid based, and powder based. The processes included in this review are considered the most relevant in the past, and promising for the future of the industry. The processes considered are stereolithography (SL), Polyjet, fused deposition modeling (FDM), laminated object manufacturing (LOM), 3D printing (3DP), Prometal, selective laser sintering (SLS), laminated engineered net shaping (LENS), and electron beam melting (EBM). The liquid-and powder-based processes seem more promising than solid-based processes of which LOM is the predominant one today." [2]

Powder bed systems operate using a directed energy source, typically a laser or, in rarer cases, an electron beam, to supply energy in the form of heat at a specific point. This energy source is directed at a bed of metal powder. This allows for the powder particles to fuse together in a controlled environment. As a layer of powder is completed, additional powder is pushed on top of the previous layer by means of a roller or rake. The laser is then used to scan the desired print pattern onto this layer, while also fusing it to the previous layer below. This process continues until the desired part is finished. [1] Figure 1 shows a breakdown of most current metal additive manufacturing processes.

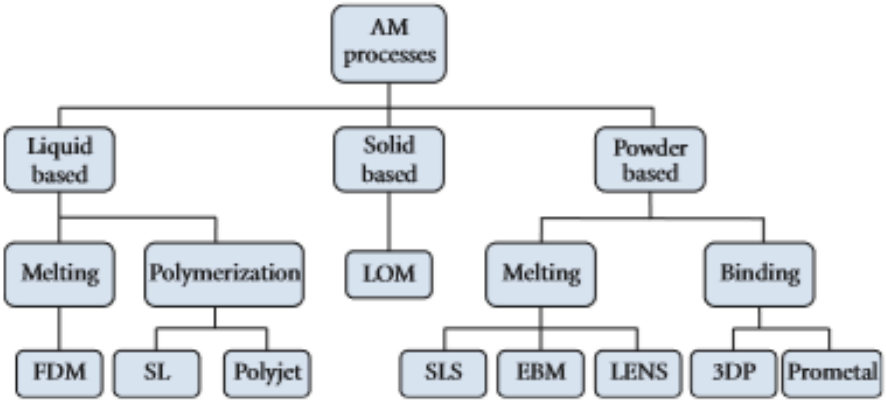

Figure 1: Breakdown of Additive Manufacturing Technologies [2]

Powder bed systems provide many desirable advantages that makes them appealing to both industry and researchers alike. For example, powder bed systems allow for complex internal features, as well as high levels of detail and control. [1] However, there are disadvantages associated with powder bed systems as well. These machines are costly to purchase as well as to operate, due to both the precise and complex laser system need and the expense of the metal powder these systems use. A large amount of powder is required to fill the build area of the bed as well, and any excess powder not used in the actual part is unable to be used again, causing

additional cost and waste of material. Also, fabricating a part with powder bed systems is slow due to the low material deposition rates provided by this process. [3] These factors inhibit powder bed systems from being employed in more widespread applications. Pictured below in Figure 2 is a common set up for powder bed systems.

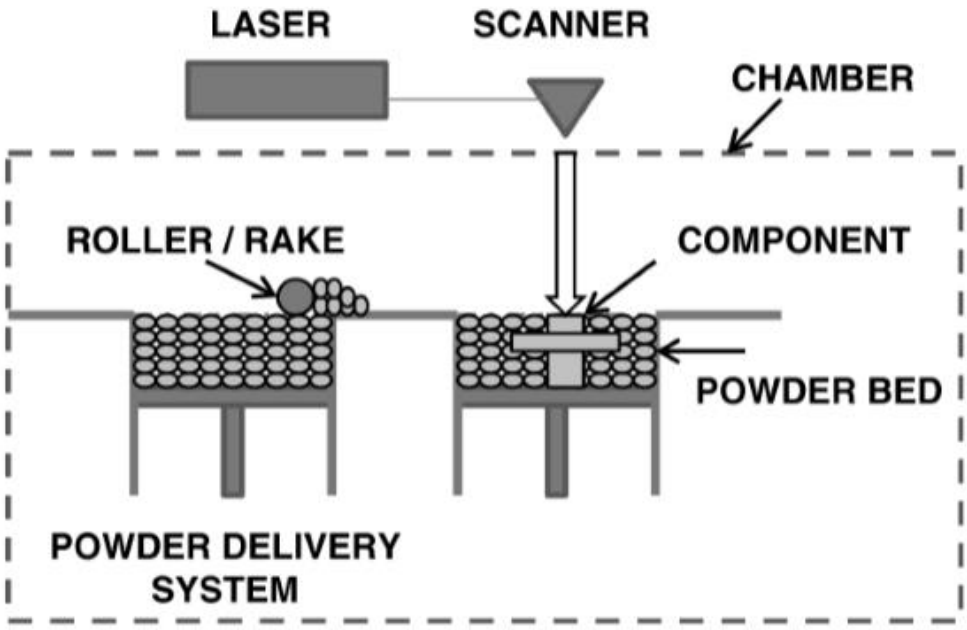

Figure 2: Powder Bed System [1]

Powder bed systems are also highly dependent on the geometry or path of the laser's scan pattern. "During production, the laser executes a scanning or exposure strategy. The strategies associated with the laser path are characterized by the length, direction, and separation (hatch spacing) of neighboring scan vectors…Scanning strategies can affect the properties of the part including density, mechanical properties, and residual stress. Residual stress is one of several important material responses that need to be optimized for laser-based additively manufactured parts. A part can be fabricated within tolerances only to have residual stress-induced distortions

put the part out of tolerance when removed from the build plate. Residual stresses can also cause a part's connection to support structures to fail or result in surface deformation" [4] While this issue is not unique to powder based systems, the laser based fusion process allows for easier identification and analysis of it.

Powder feed systems also use powdered metal to produce a part, but unlike powder bed methods, the energy is not directed onto the powder. Rather, the powder is fed into the build space along with the energy source. The metal powder then melts as it is being deposited in layers. This is often accomplished by feeding the powder through a nozzle that deposits the metal into the energy beam, and then onto the build area. [1] Figure 3 below details a standard powder feed set up.

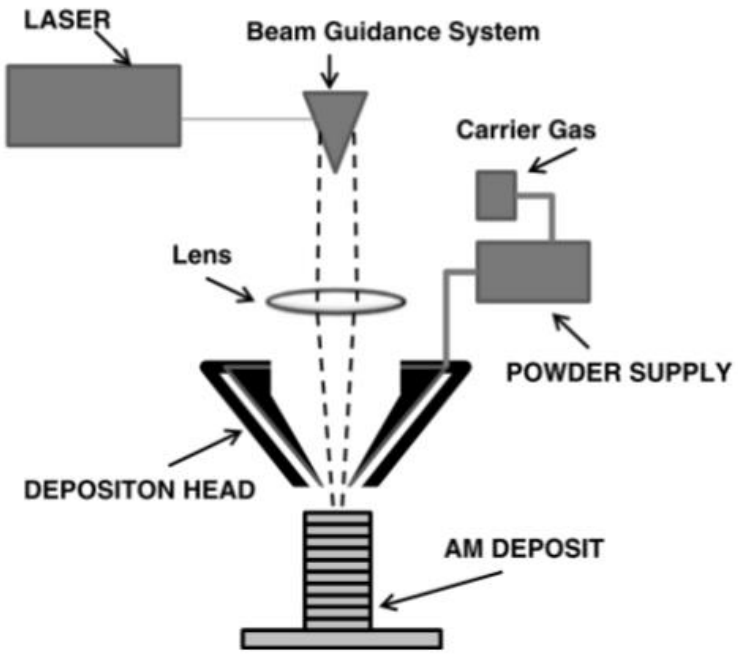

Figure 3: Powder Feed System [1]

Both powder feed and powder bed systems require highly engineered materials to operate as well. “[A] number of challenges remain including contamination issues, chemistry control during the melting process and solidification cracking, amongst others. Resulting AM parts must meet desired specifications for chemistry, surface roughness, damage tolerance, fatigue, strength, and other properties that may be sensitively affected by subtle changes to the chemistry and/or resulting microstructure and defect population.”[5]

Powder feed systems have many similarities to powder bed systems, especially in advantages and disadvantages. One key difference, however, is that powder feed systems are not as capable at providing the high detail internal features that powder bed systems can. Powder bed systems are able to make repairs to damaged parts, which is an advantage unique to this method. [2]

Wire fed systems classify a wide range of additive manufacturing methods that utilize metal wire fed into the build area. An energy source is used to melt the wire and deposit it at the build point. This process is repeated layer by layer to build the desired part. [1] Many subcategories of wire fed systems exist to meet different applications, but the base method stays the same amongst them. Wire fed systems offer “high deposition rate processing and have large build volumes; however, the fabricated product usually requires more extensive machining than the powder bed or powder fed systems do”. [1]

While the need for additional post-processing with most parts made using wire feed systems can limit its use in many applications, the cost reduction and speed allow for rapid prototyping capabilities to determine general information and characteristics about the designed part. Figure 4 demonstrates a typical wire fed system.

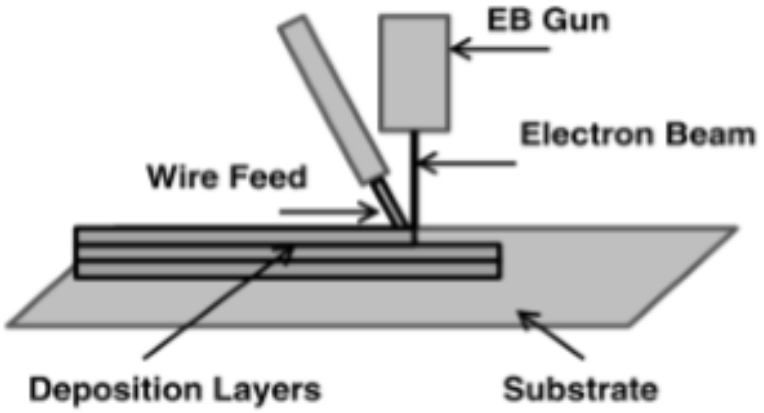

Figure 4: Wire Feed System [1]

Wire Additive Manufacturing:

Previously, wire additive manufacturing could be broken down into two major categories: Tungsten Inert Gas (TIG/GTAW) or Metal Inert Gas (MIG/GMAW). [6] Depending on which welding set up was used, a wire additive manufacturing system would be classified as one of these two set ups.

"The TIG process uses an energy source (laser, electron beam, or electricity) to melt a fed wire in an inert gas environment. The MIG process uses a consumable wire electrode that is melted by electricity and deposited in an inert gas environment."[7] While the operation of these two systems is similar in many ways, there are still key differences, advantages, and disadvantages to each. TIG additive manufacturing systems offer better control of the electrical arc, and a superior surface finish when the part is completed. MIG systems however have fewer moving parts, as the electrode and the deposited metal are the same object, and consequently is easier to maintain during the build cycle. [7]

Deposition Paths in Wire Additive Manufacturing:

Deposition paths or deposition geometries refer to the path the print head or material deposition source takes when placing material in wire based additive manufacturing. Deposition can play a major role in determining final material properties and characteristics of the part produced. Song, et al, recorded and analyzed experimental data on deposition geometries as part of his teams' research into parametrization of 3D welding processes. During this process, several different paths were utilized to build test samples. Figure 5 shows examples of potential deposition geometries.

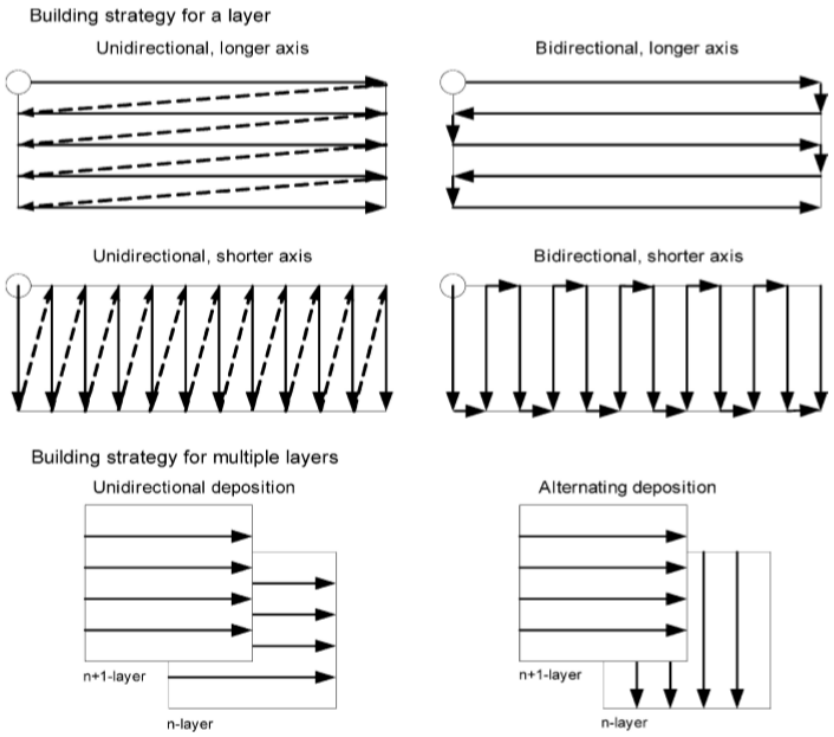

Figure 5: Deposition Geometries for 3D Welding [8]

Their experiments involved depositing a single bead of material in these different patterns. The key parameters they identified were the offset of the bead, the direction of material deposition

in each layer and the direction of material deposition between layers. [8] After these parameters were identified, and experimental data was recorded, determinations were made as to which material properties were the most effected. “According to the ANOVA, the deposition parameters hardly affect the surface hardness, while the alternating deposition direction between layers has the highest influence on the tensile strength with a percent contribution of 97.7%...Compared to this, the influence of the other deposition parameters on the tensile strength is relatively low, with a percent contribution of 1.66% for bead offset and 0.035% for deposition direction within the layer.” [8] Figure six displays the resulting deposition geometries within test specimens.

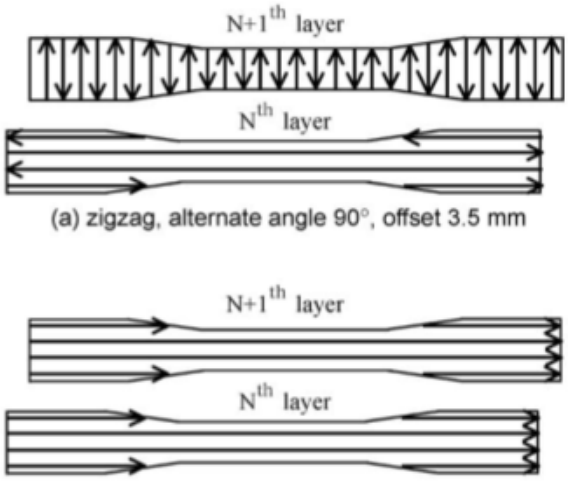

Figure 6: Deposition Geometries in Test Specimens [8]

Ultimately, Song, et al., determined that the best geometry for parts made by 3D welding was alternating by 90° between each layer, as the parts are likely to experience loading in multiple directions. They also cited the alternating deposition as eliminating voids in the last layer deposited. [8] Further, they employed a 3.5mm offset and a zigzag deposition pattern within the individual layers. No indication was given that this method was significantly superior to the others tested.

In conjunction with Rolls-Royce Corp., Clark, et al., conducted a similar analysis to determine the potential implementation of welding based additive manufacturing, or shaped metal deposition as it was referred to in their work. Their research was analyzing welding additive manufacturing for a particular specialty nickel superalloy known as Alloy 718 used for aerospace engines. Once again, deposition patterns were studied. Several different paths were taken, including single beads with multiple layers, multiple beads with single layers, and multiple beads with multiple layers. The final result of this research showed that both cooling and deposition patterns played important roles in the success of the print. [9]

Induction Heating:

Induction heating dates back to 1831, when Michael Faraday experimented with electromagnetic induction by running alternating current through two wire coils. [10] Since then, further development and experimentation was performed to increase the functionality of this process. The phenomenon that cause heating to occur in induction heating are Joule heating energy losses, and magnetic hysteresis. [10] These are achieved by running an alternating current through a copper coil, which creates a magnetic field. When an electrically conductive material is placed within this field, small electrical currents, called eddy currents, are generated within the magnetic piece. The flow of these eddy currents in the magnetic material causes heating. The three breakdowns of induction heating based on frequency are low frequency, which is less than 1 kHz, medium frequency, which ranges from 1 to 50 kHz, and high or radio frequency, which is greater than 50 kHz. [10] Figure 7 below illustrates the resulting magnetic field from an induction coil.

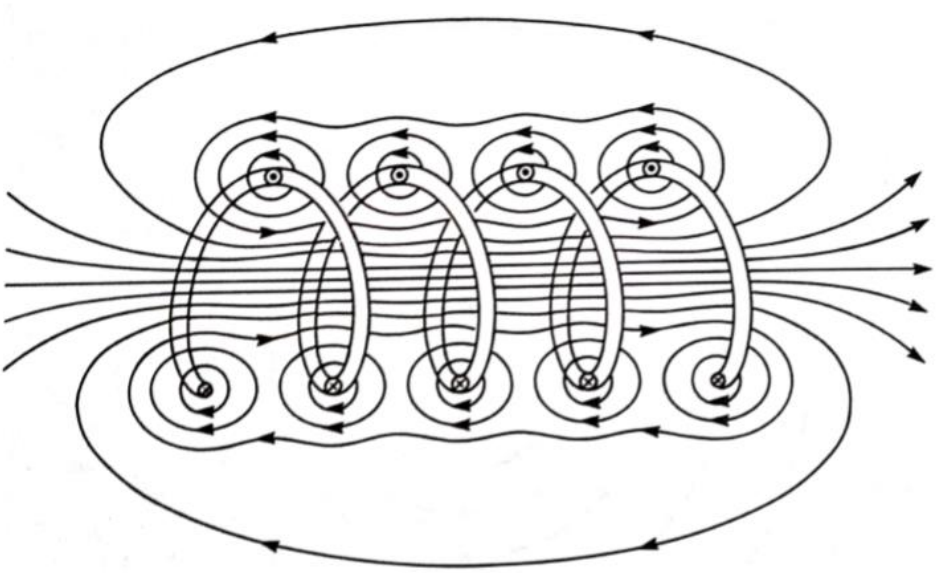

Figure 7: Illustration of Magnetic Field Created by an Induction Coil [10]

Induction heating offers many advantages that other heating systems cannot provide including:

- " Quick heating. Development of heat within the workpiece by induction provides much higher heating rates than convection and radiation processes that occur in furnaces. "[10]
- "Less scale loss. Rapid heating significantly reduces material loss due to scaling (e.g, for steels) relative to slow gas-fired furnace processes." [10]
- "Fast start-up. Furnaces contain large amounts of refractory material that must be heated during start-up, resulting in large thermal inertia. The internal heating of the induction process eliminates this problem and allows much quicker start up." [10]
- "Energy savings. When not in use, the induction power supply can be turned off because restarting is so quick. With furnaces, energy must be supplied continuously to maintain, temperature during delays in processing and to avoid long start-ups." [10]

- “High production rates. Because heating times are short, induction heating often allows increased production and reduced labor costs.” [10]

In addition to these advantages, induction heating provides “Ease of automation and control…Reduced floor space requirements…Quiet, safe, and clean working conditions… [and] Low maintenance requirements.” [10] Over the years, many applications for induction heating have been developed, including heat treating, welding and brazing, coating, bonding, casting, and more. [10, 11]

Induction Casting:

Metal casting covers a broad range of methods used to shape molten metal is it freezes. Many techniques to heat the metal are employed. In induction casting, a coil is used to provide heat to a furnace using one of two layouts: coreless or channel. [10, 11] This process is called induction casting or induction melting.

Coreless induction furnaces rely on more natural processes for their operation. This setup is simpler than channel furnace layouts. “A coreless induction melting furnace consists of a refractory envelope to contain the metal surrounded by the coil. When the metal is molten, agitation occurs naturally. This stirring action is directly proportional to the square root of the frequency…. Coreless furnaces are classified according to the frequency of the AC power supply. The important types are line-frequency (50/60 Hz) and medium-frequency (180 Hz to 10 kHz) units. The line-frequency furnace is primarily used for high-tonnage applications (3-40 tons), whereas medium-frequency equipment finds its greatest use in applications ranging up to 5 tons.” [10] Coreless induction offers its own set of unique features for applicable melting operations. Below in Figure 8 is an example illustration of a coreless induction furnace.

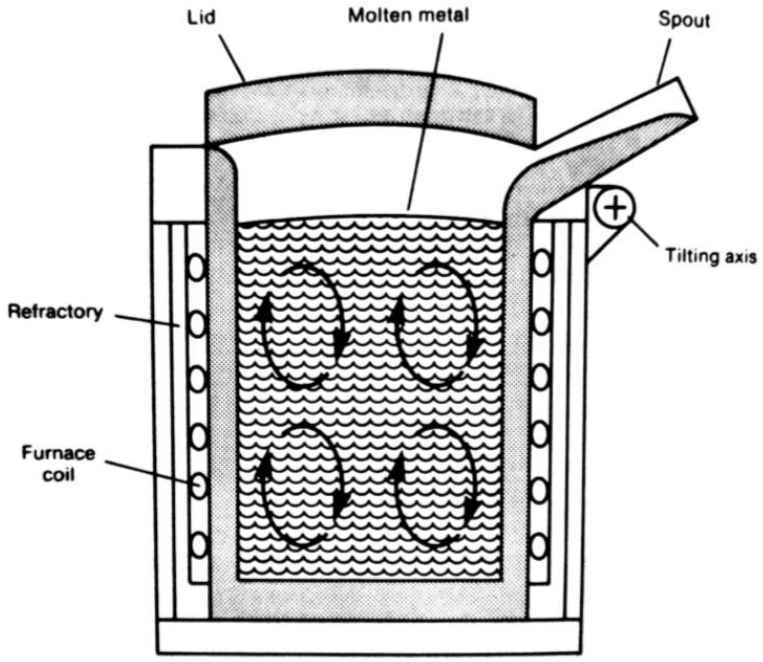

Figure 8: Coreless Induction Furnace [10]

Coreless induction furnaces are also known as crucible type. [11] By using a coreless induction furnace, several advantages are offered, such as, “increased coil efficiency when melting low resistive metals…precise temperature control…lower capital and installation costs…[and] maximum alloy flexibility.” [11]

“Channel induction melting furnaces are primarily of the line frequency type. The inductor in this design consists of a coil fitting over the core of magnetic steel laminations. The essential feature of the construction of the furnace is thus a small channel in the refractory vessel which surrounds the coil. This channel forms a continuous loop with the metal in the main part of the furnace body. By convection, the hot metal in the channel circulates into the main body of the charge in the furnace envelope to be replaced by colder metal. Unlike coreless induction melting,

a source of primary molten metal is always required for start-up of the channel furnace." [10] Figures 9 and 10 provide a view at coreless and channel induction furnaces.

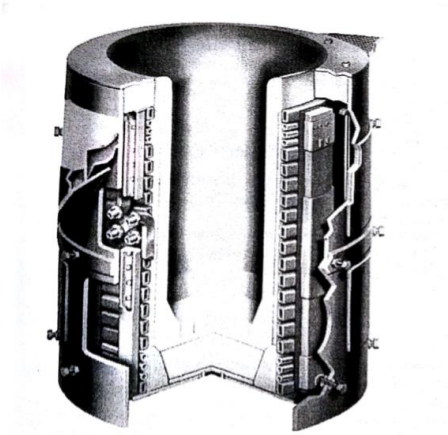

Figure 9: Sketch of Inductotherm's Coreless Furnace [11]

Channel furnaces are well suited for high-volume continuous use, especially when used in conjunction with other furnaces. [11] These furnaces are less flexible than coreless but offer the ability to process high amounts of material.

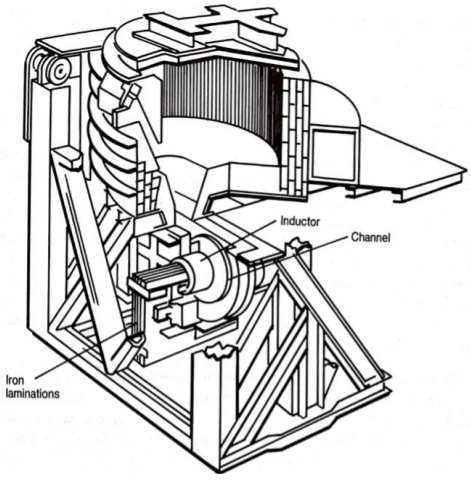

Figure 10: Channel Induction Furnace [10]

Material Properties and Induction Heating:

The effects of induction heating vary based on the material that is being heated using this process. Electrical resistivity, symbolized by ρ, plays a role in how well a metal responds to the induction process. Joule heating, also known as resistive heating, is the process by which the eddy currents created by the magnetic field heat the object inside the induction coil. Joule Heating is proportional to the current squared multiplied by the resistance. The resistance of an object, R, is also directly proportional to the resistivity, ρ. This means that as the higher the resistivity of a material, the more easily it will be heated by Joule heating, and in turn, the more quickly it will respond to induction heating. Table 1 below lists several materials' electrical resistivities.

Table 1: Electrical Resistivities of Some Common Materials [11]

Material (at Room Temperature)	Electrical Resistivity (μΩ * m)	Material (at Room Temperature)	Electrical Resistivity (μΩ * m)
Silver	0.015	Stainless Steel	0.7
Copper	0.017	Lead	0.21
Gold	0.024	Titanium	0.42
Aluminum	0.027	Nichrome	1
Tungsten	0.054	Graphite	14,000
Zinc	0.059	Wood	10^14—10^17
Nickel	0.068	Glass	10^16—10^20
Cobalt	0.09	Mica	10^17—10^21
Mild carbon steel	0.16	Teflon	>10^19

Another material property to be considered in induction heating is the relative magnetic permeability. This is the "ability of a material to conduct the magnetic flux better than a vacuum or air." [11] Similarly related to this is the relative permittivity, or dielectric constant. This is "the ability of a material to conduct the electric field better than a vacuum or air." [11] Both of these properties factor into how the electromagnetic field created by the induction coil will interact with

the material. Materials can be classified based on their magnetic permeability. The three classifications are paramagnetic (magnetic permeability slightly greater than 1), diamagnetic (magnetic permeability slightly less than 1), and ferromagnetic (magnetic permeability much great than 1). [11]

Skin Effect:

Several factors are important in the consideration of induction heating, but perhaps the most important is known as the skin effect. The skin effect is the determination of the depth to which the eddy currents will penetrate the material being heated by the induction coil. "[W]hen an alternating current flows through the same conductor, the current distribution is not uniform…This phenomenon of nonuniform current distribution within the conductor cross-section is called the skin effect, which always occurs when there is an alternating current. Therefore, the skin effect will also be found in the workpiece located inside an induction coil…Due to the circumferential nature of the eddy current induced in the workpiece, there is no current flow at the center of the workpiece…Because of this effect, approximately 86% of the power will be concentrated in the surface layer of the conductor" [11] Figure 11 demonstrates the current distribution in an induction workpiece.

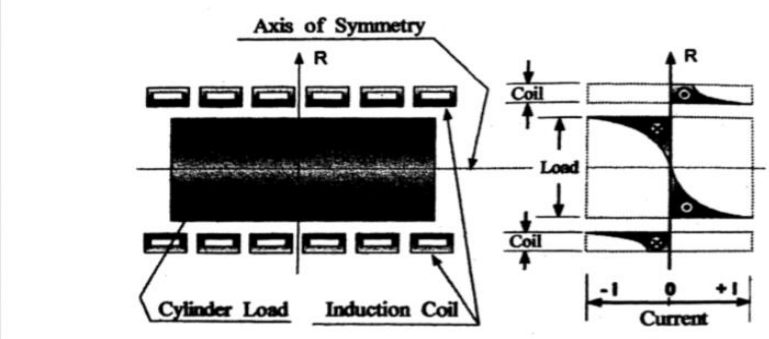

Figure 11: Current Distribution in "coil-workpiece" induction system [11]

The penetration depth is the layer in which approximately 86% of the power is concentrated, and is designated using the symbol δ. [11] Penetration depth can be calculated in both inches and meters as

$$\delta = 3160\sqrt{\rho/\mu_r F'} \quad (1)$$

$$\delta = 503\sqrt{\rho/\mu_r F'} \quad (2)$$

where ρ is the electrical resistivity of the material, μ_f is the magnetic permeability, and F' is the freqency. Since two of these values are constant based on the material chosen for the workpiece, penetration depth can be calculated for any given material across an array of frequencies. Valery Rudnev et al. did so in *Handbook of Induction Heating*. Tables 2 and 3 provide the penetration depts for nonmagnetic materials and carbon steel respectively.

Table 2: Penetration Depth of Nonmagnetic Metals (mm) [11]

	T		*ρ*		Frequency (kHz)										
Metal	°C	°F	μΩ · m	μΩ · in.	0.06	0.50	1	2.5	4	8	10	30	70	200	500
Aluminum	20	68	0.027	1.06	10.7	3.70	2.61	1.65	1.30	0.92	0.83	0.48	0.31	0.18	0.12
	250	482	0.053	2.09	15.0	5.18	3.66	2.32	1.83	1.29	1.16	0.67	0.44	0.26	0.16
	500	932	0.087	3.43	19.2	6.64	4.69	2.97	2.35	1.66	1.48	0.86	0.56	0.33	0.21
Copper	20	68	0.018	0.71	8.81	3.05	2.16	1.36	1.08	0.76	0.68	0.39	0.26	0.15	0.10
	500	932	0.050	1.97	14.5	5.03	3.56	2.25	1.78	1.26	1.12	0.65	0.43	0.25	0.16
	900	1,652	0.085	3.35	19.3	6.67	4.72	2.98	2.36	1.67	1.49	0.86	0.56	0.33	0.21
Brass	20	68	0.065	2.56	16.6	5.74	4.06	2.56	2.03	1.43	1.28	0.74	0.48	0.29	0.18
	400	752	0.114	4.49	21.9	7.60	5.37	3.40	2.69	1.90	1.70	0.98	0.64	0.38	0.24
	900	1,632	0.203	7.99	29.3	10.1	7.17	4.53	3.58	2.53	2.27	1.31	0.86	0.51	0.32
Stainless steel	20	68	0.690	27.2	53.9	18.7	13.2	8.36	6.61	4.67	4.18	2.41	1.58	0.93	0.59
	800	1,472	1.150	45.3	69.6	24.1	17.1	10.8	8.53	6.03	5.39	3.11	2.04	1.21	0.76
	1,200	2,192	1.240	48.8	72.3	25.1	17.7	11.2	8.86	6.26	5.60	3.23	2.12	1.25	0.79
Silver	20	68	0.017	0.67	8.34	2.89	2.04	1.29	1.02	0.72	0.65	0.37	0.24	0.14	0.09
	300	572	0.038	1.50	12.7	4.39	3.10	1.96	1.55	1.10	0.98	0.57	0.37	0.22	0.14
	800	1,472	0.070	2.76	17.2	5.95	4.21	2.66	2.10	1.49	1.33	0.77	0.50	0.30	0.19
Tungsten	20	68	0.050	1.97	14.5	5.03	3.56	2.25	1.78	1.26	1.12	0.65	0.43	0.83	0.53
	1,500	5,072	1.550	21.7	48.2	16.7	11.8	7.46	5.90	4.17	3.73	2.15	1.41	0.83	0.53
	2,800	5,072	1.040	40.9	66.2	22.9	16.2	10.3	8.11	5.74	5.13	2.96	1.94	1.15	0.73
Titanium	20	68	0.500	19.7	45.9	15.9	11.3	7.11	5.62	3.98	3.56	2.05	1.34	0.80	0.50
	600	1,112	1.400	55.1	76.8	26.6	18.8	11.9	9.41	6.65	5.95	3.44	2.25	1.33	0.84
	1,200	2,192	1.800	70.9	87.1	30.2	21.3	13.5	10.7	7.54	6.75	3.90	2.55	1.51	0.95

Table 3: Penetration Depth of Carbon Steel 1040 at Ambient Temperature 21°C (70°F) [11]

Magnetic Field Intensity		Frequency (Hz)											
		60		500		3,000		10,000		30,000		100,000	
		Penetration Depth											
A/mm	A/in.	mm	in.	mm	in.	mm	in.	mm	in.	mm	in.	mm	in.
10	250	2.50	0.100	0.88	0.034	0.36	0.014	0.2	0.008	0.11	0.004	0.06	0.002
40	1000	4.70	0.185	1.63	0.064	0.67	0.026	0.36	0.014	0.21	0.008	0.12	0.005
80	2000	6.30	0.249	2.20	0.086	0.9	0.035	0.49	0.019	0.28	0.011	0.16	0.006
160	4050	8.76	0.345	3.03	0.119	1.24	0.049	0.68	0.027	0.39	0.015	0.21	0.008
200	5100	9.63	0.379	3.33	0.131	1.36	0.054	0.75	0.029	0.43	0.017	0.24	0.009
280	7100	11.20	0.442	3.89	0.153	1.59	0.062	0.87	0.034	0.50	0.020	0.27	0.011

The magnetic field intensity, H can be found using the equation

$$H = \frac{NI}{l} \tag{3}$$

where N is the number of turns, I is the coil current in amps, and l is the length of the solenoid. [11] From here, the skin depth can be determined using the penetration depth tables above for different conditions. The heating of induction is done through eddy currents traveling through the workpiece by means of resistance heating. The heat generation in an induction coil can be modeled using

$$c\gamma \frac{\partial T}{\partial t} + \nabla * (-k\nabla T) = Q \tag{4}$$

Due to the complexity of this equation, it is recommended that this is solved using simulation software, such as ANSYS, SolidWorks, or another computational software. [11] The axial magnetic field, B_z, is another valuable characteristic that can be approximated by

$$B_z = \frac{\mu_0 NI}{2l} \tag{5}$$

where μ_0 is the magnetic permeability, N is the number of turns, I is the current, and l is the solenoid length.

One other aspect to consider is the workpiece power, P_w, expressed by the equation

$$P_w = mc\frac{T_f - T_{in}}{t} \quad (6)$$

where m is mass, c is specific heat, T_f is the final temperature, T_{in} is the initial temperature, and t is the time. These values are useful in consideration of the design of the crucible so as to allow quick and consistent melting of the desired material.

Aluminum Casting:

Aluminum casting is a common practice to net shape aluminum by use of filling a mold. This is due in large part to the wide range of uses for aluminum and the ease of casting it. [12] When casting, there are several material characteristics that are important to the casting process. The characteristics that are sought after in casting aluminum include:

1. "Good fluidity—flows relatively easily through narrow passages or orifices." [12]
2. "Low melting point—compared to other materials in its group." [12]
3. "Beneficial solidification range—the differential between temperature at which solidification begins and the temperature at which it is completed." [12]
4. "Low gas solubility—the dissolving of gases in the molten metal." [12]
5. "Not hot shortness—the fracture tearing of a metal during solidification." [12]
6. "Good chemical reproducibility and alloying efficiency—the ease with which chemical composition can be held within specified limits." [12]
7. "Good as-cast surface finish—no surface pitting or heavy adhering scale." [12]

All of these factors are important to consider when selecting an alloy for the casting process.

Another advantage to casting aluminum is that there are a wide array of methods that can be utilized. Most forms of casting involve the use of some type of mold. Typically, these molds fall under one of two main types, sand casting and some type of permanent mold casting. [12] Sand casting is by far the most prevalent form of metal casting currently used in industry, based on the total tonnage of castings. [13]

Sand casting can be further broken down into several subcategories, such as green sand casting, sand casting with a chemical binder, sand casting using oil binders, and sand casting with Styrofoam molds. [13] These different methods are used for various applications based on the need of the part being cast.

Green sand is a term applied to a process that utilizes water in the casting medium in addition to the sand. This typically uses a two-part flask filled with green sand set up to allow molten metal to fill it. Weights can be utilized to prevent separation of the two halves during the pouring process. The metal will solidify in the mold and then be removed. For this process, sand is not the best choice, but clay is often a desirable replacement. [13]

"Green sand casting is not difficult and it is not too expensive to get started. Molten metal is taken from a furnace and poured into a sand mold. The sand in the mold is held together by a binder such as clay and a little water to make a damp sand or green sand mold. The mold is made by packing molding sand around a pattern or duplicate of the part to be cast. A flask holds the sand around the pattern. Once the sand is packed or 'rammed' around the pattern, the mold is opened and the pattern is removed. If required, and cores are set into place. The mold is closed and the molten metal is poured into a basin or pouring cup. It flows through a hold made in the sand called a sprue. The molten metal flows into the mold cavity through a gate. After the metal has cooled,

the casting is removed from the sand, cleaned and finished." [14] Figure 12 provides a visual aid of the sandcasting process.

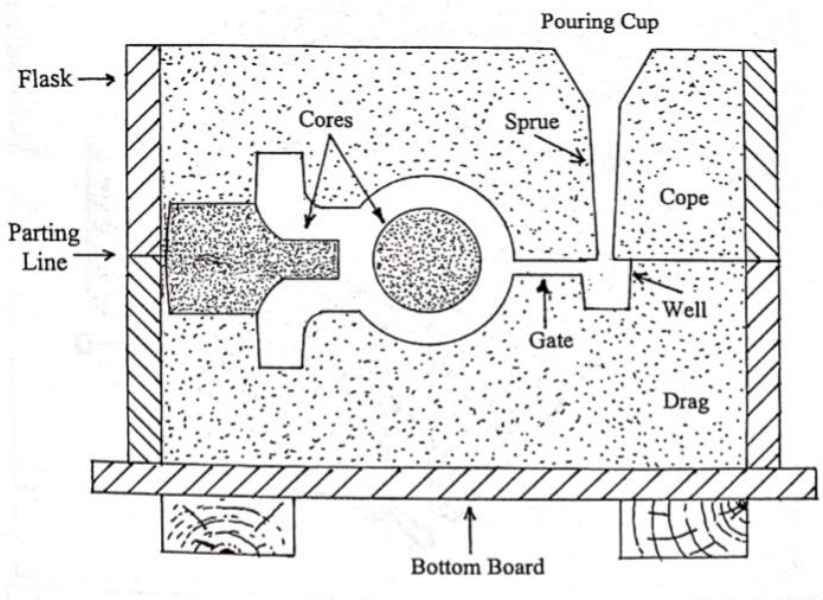

Figure 12: Sand Casting Mold Illustration [14]

Sand casting with chemical binders and oil binders are similar overall in the processes used. In both cases, silica sand is mixed with some type of binder, whether it is a chemical catalyst or a commercial drying oil. [13] Casting with Styrofoam molds uses a piece or multiple pieces of Styrofoam to create the net shape desired. It is then placed down into the sand, and when the metal is poured, the Styrofoam vaporizes and the metal fills the cavity. [13]

As stated earlier, all of these methods described involve a mold to shape the molten metal to the desired form. While some moldless methods are in experimental development, little information is available about them. Most descriptions of these processes would likely fall under various additive manufacturing methods previously discussed, though it is difficult to classify due to the limited amount of research and publications regarding this topic.

Aluminum casting carries with it a number of material and mechanical constraints that must be taken into consideration. One major issue in aluminum casting is the possibility of gas porosity. “Considering first the reaction of liquid aluminium with oxygen, the solubility of oxygen in aluminium is extremely small; less than one atom in about 10^{35} or 10^{40} atoms. This corresponds to less than one atom in the whole world supply of the metal since extraction began…Oxygen can only react with the surface. Furthermore, the surface can only access the interior of the metal if it is entrained, or folded in. This is a mechanical, not a chemical process…We now turn to the presence of hydrogen in aluminium. This behaves quite differently.” [15]

Aluminum is much more susceptible to hydrogen dissolving into it while it is molten. “[O]n a normal day with 30 percent relative humidity the hydrogen level will continue to be tolerable for most applications. This is the rationale for degassing aluminum alloys by doing nothing other than waiting. If originally high in gas, the melt will equilibrate by losing gas to the environment…Raising the temperature of the melt will increase the solubility of hydrogen in liquid aluminium. At a temperature of 1000° C the solubility is over 40 $ml.kg^{-1}$. However, of course, if there is no hydrogen available in its environment the melt will not be able to increase its gas content no matter what its temperature is…[U]sually, high temperatures are best avoided if gas levels are to be kept under good control. Most aluminium alloy castings can be made successfully at casting tempeartures of 700-750°C.” [15]

Due to this issue, some method of dealing with hydrogen is necessary during the aluminum casting process. This can be accomplished by flushing the area around the cast with an inert gas, by creating an inert atmosphere enclosing the cast, or by implementing a degassing system. [15] Figure 13 plots the hydrogen content with molten aluminum’s temperature below.

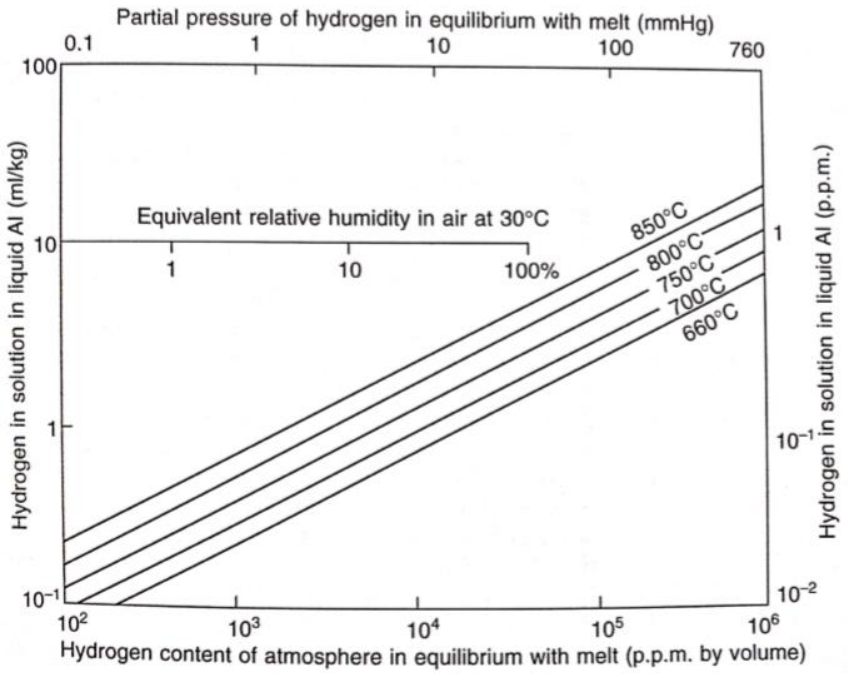

Figure 13: Hydrogen Content of Liquid Aluminum [15]

Other design constraints to take into consideration are geometrical, thermal, and mechanical conditions that are a direct result of the mold design. The development of hot spots caused by large areas of deposited material or the inclusion of sharp corners and geometric changes can lead to shrinkage cracking as the material cools and higher residual stresses form in the part. [12] By avoiding these, the part cast will have better structural integrity and be less prone to failing.

Another design constraint to be considered is the thickness of the part in the mold as it is cast. Nonuniform thickness can lead to uneven degrees of cooling and shrinking, causing uneven material properties and high stresses in different locations. [12] Figures 14 and 15 highlight potential problems and proper practices in casting.

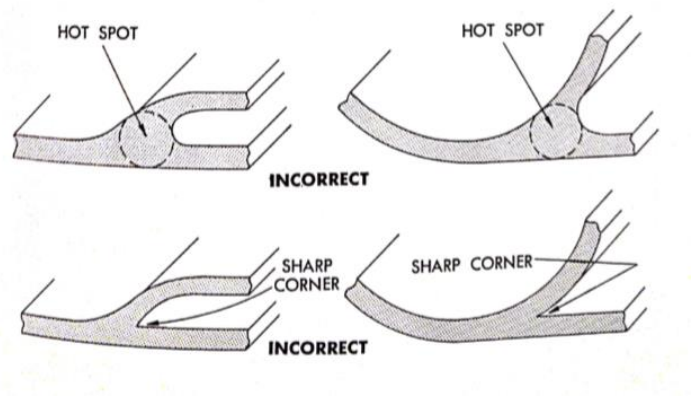

Figure 14: Demonstration of Hot Spot and Sharp Feature Developments [12]

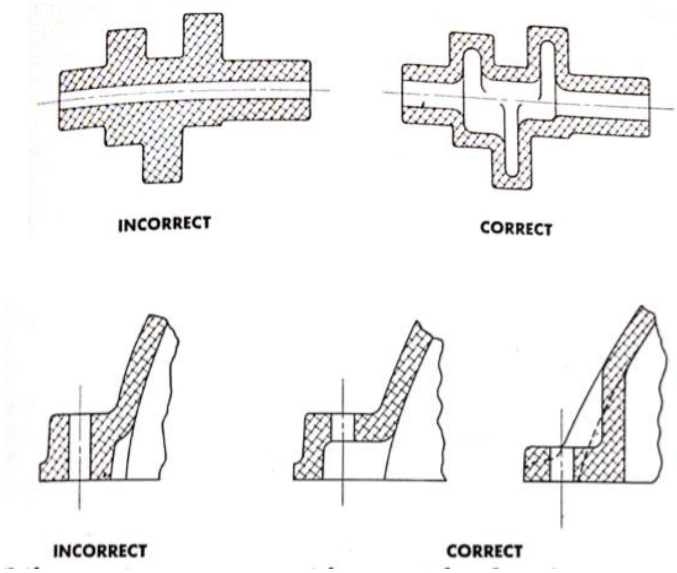

Figure 15: Designing Uniform Thickness in Casting [12]

Semi-Solid Casting:

Semi-solid casting is a special form of casting that involves keeping a metal from fully reaching its melting point. Some metals, such as aluminum, copper, and magnesium, respond more readily to this process. “Semi solid metal(SSM) processing, also known as semisolid metal casting, semisolid forming, or semisolid metal forging, is a special die casting process wherein a partially solidified metal slurry (typically, 50% liquid+50% solid instead of fully liquid metal) is injected

into a die cavity to form a die-cast type of component." [16] While a 50% liquid 50% solid mixture is the most common, these values can range from anywhere between 25% and 75% of either liquid or solid.

This process allows for several advantages that traditional casting methods do not provide. Semi-solid casting was first developed by David Spence while conducting his doctoral research at Massachusetts Institute of Technology. [16] Through his research, he found that a slurry of partially solidified metal would behave with many characteristics of a solid, but was capable of flowing like a liquid when subjected to a shear force. [16] Due to the relatively low viscosity of the metal in this state, a constant flow can be produced to deposit the metal in a uniform manner.

Rheocasting and thixocasting are other names for specific methods of semi-solid casting, based on heating and freezing of the metal as well as its properties. Thixocasting utilizes pre-cast billet with a particular microstructure, and reheats the metal to a semi-solid state. [17] Rheocasting, however, creates the semi-solid state in a separate machine from the actual casting machine from the liquid state, and then injects it into a die. The semi-solid state of the metal is created directly from the molten material. [17] Figure 16 breaks down the steps of the rheocasting process.

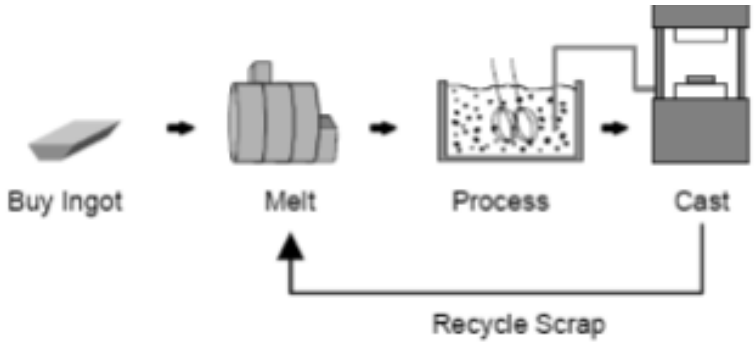

Figure 16: Rheocasting Process [17]

"Thixoforming is a viable technology for forming alloys in semisolid state to near net-shaped products. Thixoforming basically consists of three phases…(a) producing a material with a globular microstructure, (b) heating the material to the forming temperature, and (c) forming the material in a die-casting press. The process relies on the thixotropic behavior of alloys with a spheroidal rather than a dendritic microstructure in semisolid state…In thixotropic condition, an alloy decreases in viscosity if it is sheared but it will thicken again if it is allowed to stand…This process requires uniform heating and partial remelting of the alloy slug to obtain a homogeneous consistency throughout." [18] The globular microstructure that is formed then is best created by interrupting the dendritic microstructure that freezes during a standard solidification process. [19] By interrupting the freezing process, the dendrites will break into a more chaotic arrangement, that then freezes into the desired globular microstructure best suited for semi-solid processes. Figure 17 demonstrates typical dendritic formation in metals.

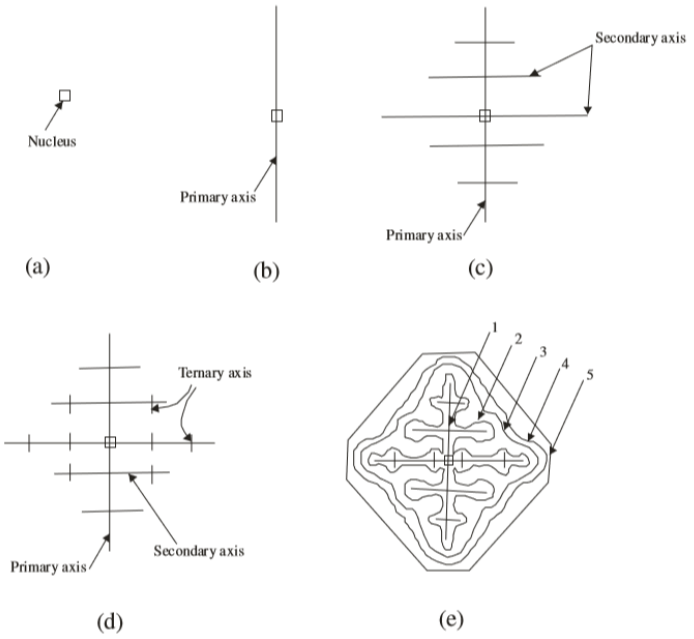

Figure 17: Development of Dendritic Microstructure [19]

The introduction of shear forces on the molten material can also play a role in disrupting dendritic formation and causing the globular or spheroidal shape to occur. “[I]n the early stages of solidification, as it happens for all metallic materials, dendrites form in the liquid. However, unlike conventional solidification, the shearing action affects the dendritic morphology, which changes into that of a “rosette” due to different phenomena. Various explanations about the conversion mechanisms from dendritic to globular morphology can be found in the literature like ripening, shear, bending and abrasion with other growing crystals, dendrite fragmentation, remelting of dendrite arms, and growth control mechanisms.” [20] The time allowed for the freezing process factors in as well. By decreasing the rate of freezing, increasing the time taken to freeze, and introducing shear force to the molten metal the development of semi-solid slurry can be more controlled. Figure 18 demonstrates globular microstructure’s formation in the semi-solid process through refreezing, while Figure 19 shows the formation process through shear force.

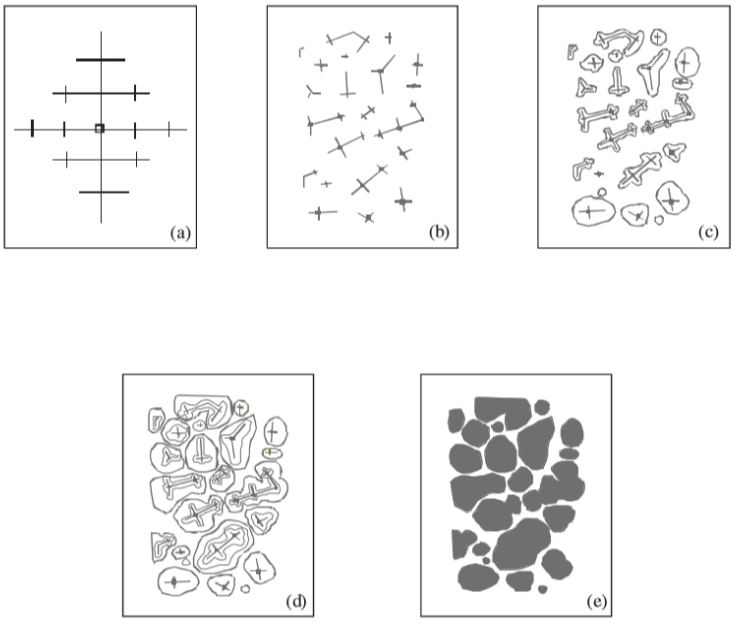

Figure 18: Development of Globular Microstructure By Interrupting Dendritic Freezing [19]

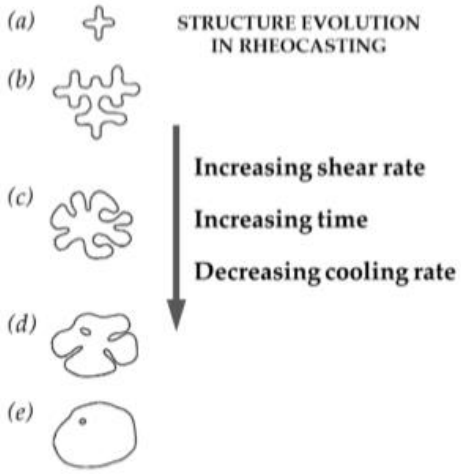

Figure 19: Development of Globule in Semi-Solid Slurry [20]

While semi-solid casting can be a difficult process, the benefits seen in the parts produced are quite noticeable. The mechanical properties of parts produced by semi-solid casting are typically stronger than parts produced by competing methods. Stephen Midson outlined the positive mechanical property advantages produced by semi-solid casting. In his research, he chose specific aluminum casting alloys and compiled data on the mechanical properties of them based on research performed by other groups. Reviewing this data shows that the semi-solid freezing process allows for higher strength materials. Tables 4, 5, and 6 compare the material properties for semi-solid and traditional casting methods for aluminum.

Table 4: Mechanical Property Data for Alloy A356 [21]

Process	**Temper**	**0.2%YS (MPa)**	**UTS (Mpa)**	**Elong. (%)**
Rheocast	T5	180	270	7
Rheocast	T6	235	310	13
Sand	T6	207	278	6
Permanent Mold	T61	205	285	10

Table 5: Mechanical Property Data for Alloy 357 [21]

Process	**Temper**	**0.2%YS (MPa)**	**UTS (Mpa)**	**Elong. (%)**
Thixocast	T5	200	285	8
Rheocast	T6	290	345	7
Sand	T6	296	345	2
Permanent Mold	T6	295	360	5

Table 6: Mechanical Property Data for Alloy 319 and 319S [21]

Process	**Alloy**	**Temper**	**0.2%YS (MPa)**	**UTS (Mpa)**	**Elong. (%)**
Rheocast	319s	T6	340	400	8
Rheocast	319	T6	165	250	2

"Semi-solid processing guarantees higher performance than die-casting, while maintaining a number of the advantages of die-casting, such as good dimensional tolerances, high production rates, high surface quality, complex near-net-shape parts, and thin sections with very limited need of any finishing operations."[20] While semi-solid casting has not yet seen wide applications in industrial use, it is clear that the process offers several desirable attributes for casting. Better yield strengths and material properties have been recorded. This is partly due to the lower gas porosity the metal experiences in the semi-solid state. In fact, in semi-solid casting, the gas porosity can sometimes be reduced to almost non-existent levels, due to the high viscosity of the liquid in this state. [17]

Fatigue properties of semi-solid castings also outperformed castings made by competing processes. Cummins Turbo Technologies analyzed the fatigue data from these differing processes and compared them. Ultimately, the parts produced by semi-solid processes had the highest fatigue strength. [22] Figure 20 compares the fatigue strength of different casting methods.

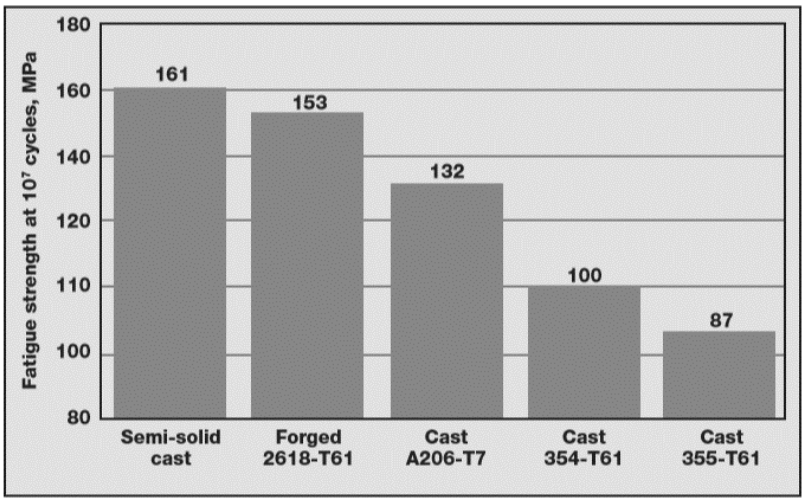

Figure 20: Comparison of Fatigue Strength for Various Casting Procedures [22]

Aluminum Extrusion:

Extrusion is a method of forming metal beginning with a billet and applying force to create plastic deformation and cause the metal to flow through an opening of the desired shape. This opening typically has a cross-sectional area smaller than the cross-sectional area of the billet. [23] "Extrusion is an indirect-compression process. Indirect-compressive forces are developed by the reaction in the workpiece (billet) with the container and die; these forces reach high values. The reaction of the billet with the container and die results in high compressive stresses that are effective in reducing the cracking of the billet material during the primary breakdown from the billet…Extrusion can be cold or hot, depending on the alloy and the method used. In hot extrusion, the billet is preheated to facilitate plastic deformation."[23] Figures 21 and 22 contrast the direct and indirect extrusion processes.

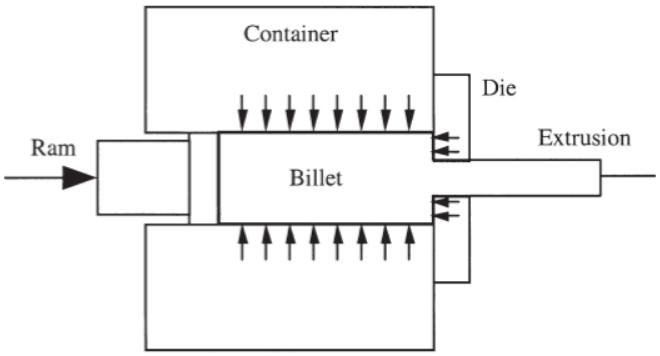

Figure 21: Illustration of Direct Extrusion Process [23]

Extrusion processes can fall under several different types. The two broad categories are direct and indirect. Direct is the most commonly employed method. In direct extrusion, a billet is loaded into a container. A ram applies force to the back of the workpiece, and the metal flows in the same direction as the ram pressing on the billet. Friction from the sides of the container increases the pressure on the workpiece. The billet is then pressed through a die, taking on the shape of the opening in the die. [23]

"In indirect extrusion, the die at the front end of the hollow stem moves relative to the container, but there is no relative displacement between the billet and the container…Therefore, this process is characterized by the absence of friction between the billet surface and the container, and there is no displacement of the billet center relative to the peripheral regions."

Several factors are necessary to take into consideration for the extrusion process, such as stresses and strains during the flow, thermal conditions, and material properties, especially potential changes throughout the metal. The primary reason these values are important is because if the pressure needed to extrude the metal becomes greater than what is able to be produced, extrusion will not be able to take place. [23]

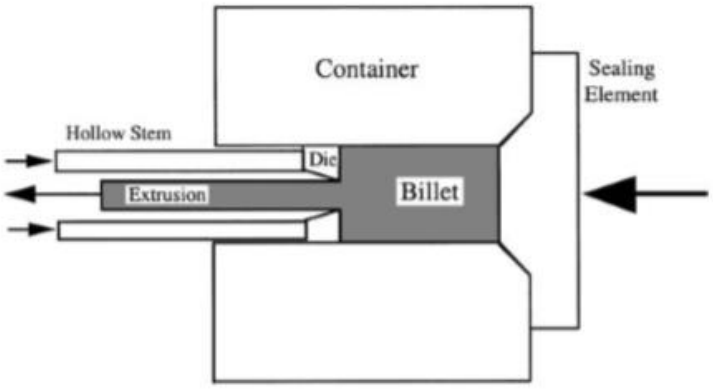

Figure 22: Illustration of Indirect Extrusion [23]

Aluminum is a desirable metal for extrusion processes, as it has many qualities that aid in its extrusion. These include that it has a good strength to weight ratio, is not prone to rusting, has good thermal conductivity, and is easily machinable. This allows for special extrusion processes to create aluminum pieces custom made for different applications. [24]

Semi-solid casting processes can be combined with extrusion to create semi-solid extrusion methods. Similar to rheocasting and thixocasting, the two most common methods of semi-solid extrusion are rheo-extrusion and thixo-extrusion. By attempting to extrude aluminum in the semi-solid state, issues that are prevalent in standard extrusion processes can be mitigated or avoided altogether, such as the amount of pressure required to extrude the material, or cracking and gas porosity. [25]

While both of these methods are still developing, rheo-extrusion has seen slightly less development, currently. Fan, et al, conducted some early studies using a screw force on aluminum alloys. A twin screw extruder setup was utilized to create laminar flow of the semi-solid material. The metal was fully melted, cooled to the semi-solid temperature range and sheared by the screws to create the semi-solid slurry. [26] This is demonstrated in the illustration below in Figure 23.

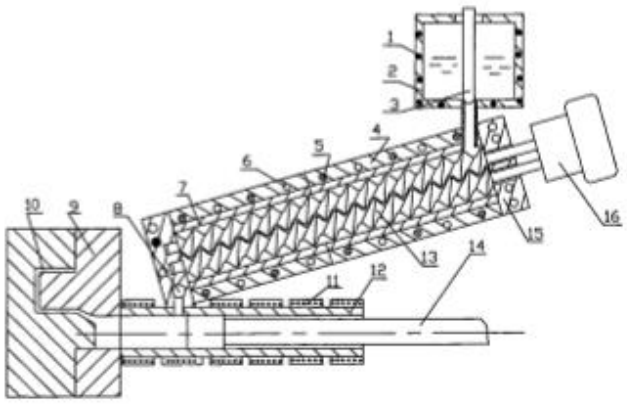

Figure 23: “Schematic illustration of the twin-screw rheomoulding process” [26]

The items number in the previous figure consist of ,” 1, Heating elements; 2, crucible; 3, stopping rod; 4, barrel; 5, heating elements; 6, cooling channels; 7, barrel liner; 8, transfer valve; 9, die; 10, mould cavity; 11, heating elements; 12, shot sleeve; 13, twin-screw; 14, piston; 15, end cup; 16, driving system.” [26]

The parts produced by this method were examined, and it was found that the microstructure of these parts were uniform and able to repeatedly produce the globular microstructure necessary for semi-solid casting. This method also allows for better control of the chemical characteristics, the range of solid volume fractions, and lowered cost. [26] Figure 24 provides a look at the resulting globular microstructure.

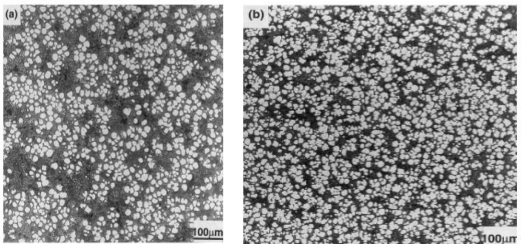

Figure 24: Microstructure of Rheo-extruded Magnesium, Detailing Globular Formation [26]

The idea of utilizing semi-solid extrusion as an additive manufacturing process was first introduced by Rice, et al., as part of his master's thesis at Massachusetts Institute of Technology. This research was then further developed into a viable process in conjunction with the US Department of Energy. At the time, Rice referred to this process as "Semi-solid metal freeform fabrication."[27] This process deposited semi-solid material in layers similar to additive manufacturing processes. The objective of Rice's research was to examine, "The feasibility of utilizing semi-solid metal freeform fabrication for the rapid production of three-dimensional Al-SI alloy parts…" [27]

Rice's setup for his research involved a multi-step system. "The deposition apparatus consists of the following: a stirring chamber for the semi-solid aluminum which also includes a heated deposition nozzle, modular heater halves to control the temperature of the semi-solid, two stirring rotors connected to their associated drive motors, a vertically sliding base on which motors are mounted, guide rails on which the sliding plate moves, a temperature controlled substrate mounted to a programmable three-axis table, and a support frame to hold each of these components." [27]

Rice utilized graphite as a stirring chamber due to the fact it would not interact with the aluminum, and had a high thermal conductivity. Two radiated heating units were outside of this chamber to control the semi-solid state, while two titanium mixing rotors inside the chamber created the shearing force necessary for globular formation. Prior to entering the stirring chamber, the metal had to be melted down and then transferred over into the stirring chamber for processing. [27] Rice's setup for his experiment is illustrated below in Figure 25.

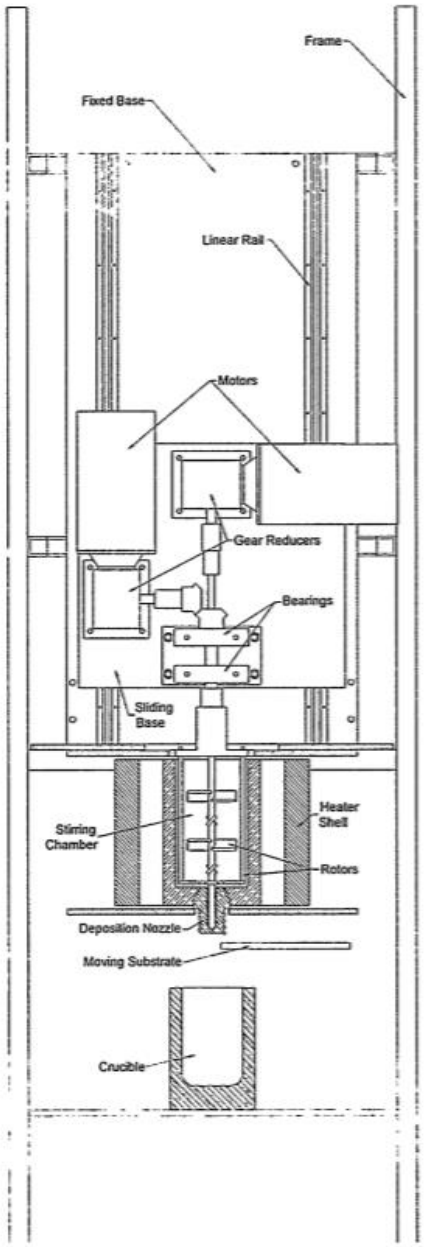

Figure 25: Illustration of Rice's Semi-Solid Freeform Fabrication Setup

Rice's research went on to analyze the deposition of the material onto the heated substrate below. He found that it was best to keep the substrate two stream diameters away from the nozzle. Distances greater than this caused the slurry to "drag", as he termed it, while at distances less than

two diameters, the deposition smeared against the nozzle. For travel rate, he utilized a speed of 20mm/sec. [27]

Rice noted that in the parts produced using semi-solid extrusion, there was significantly lower gas porosity. The low porosity could be credited to the fact that, as the material had already solidified, there was less opportunity for gases to dissolve into the metal. By controlling the cooling of the part, Rice stated that the size of particles could be more controlled as well. “The size of the primary solid particles is governed mostly by cooling (or heat extraction) rate. In the case of the present prototype, the semi-solid was held at constant temperature with little cooling, so the particles grew to 50 to 300 microns in size. Since the solid particle size represents a lower bound on the minimum stream diameter, it may be desirable to reduce their size, if possible.” [27] The resulting microstructure from Rice’s tests is shown below in Figure 26.

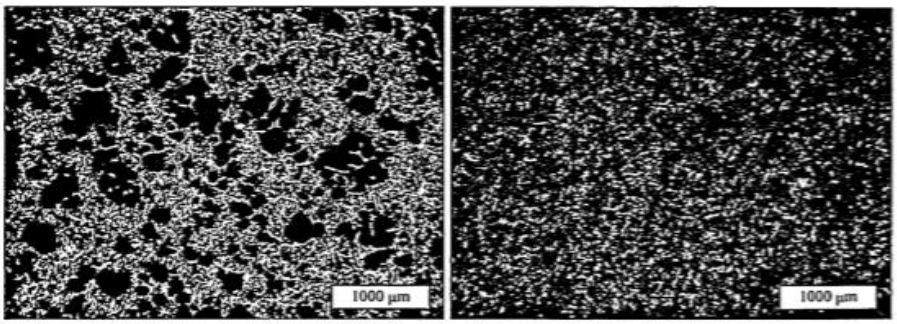

Figure 26: Microstructure of Rice’s Test Parts

Jabbari, et al., further examined the possibility of developing an additive manufacturing process based on thixo-extrusion. The goal was to achieve laminar controlled flow of the semi-solid material as it was deposited onto the build plate. Unlike rheo-extrusion, where the semi-solid slurry is created by the introduction of shear forces to the molten material, in thixo-extrusion, the metal is melted, allowed to cool, and then reheated as it is being extruded. [28]

"Considering the semisolid metal forming technologies, these approaches are classified as rheo-casting processes where the globular microstructure is obtained by imposing shear in the melt and partial solidification delivers SSM. The approach chosen in this paper is quite the opposite. In here the solid feedstock is prepared with the desired microstructure and the forming process takes place by partial re-melting of the feed stock. This process is abbreviated as SSMED and is known as thixo-forming." [28] In this study, wire feedstock was used, first going through a pretreating station, then cooling and being fed into the thixo-extruder. Inside the thixo-extruder, the wire was reheated to enter the semi-solid state, and then deposited onto the bed. Lead and tin alloys were created and pre-treated specifically for this research. Several factors were analyzed to determine which had the most bearing on the properties of the final part and the success of the print. Nozzle diameter and feed rate were found to be two of the most important variables in this study, and data was collected at different values for each of these.[28] Table 7 below compares the shear rate and apparent viscosity in these experiments.

Table 7: Shear Rate and Apparent Viscosity from Jabbari's Study [28]

	Feed Rate	2mm/s	5mm/s	10mm/s	20mm/s
1mm Nozzle	Shear Rate (S^-1)	198	495	N/A	N/A
	App Viscosity (Pa.s)	1.9	1.1	N/A	N/A
2mm Nozzle	Shear Rate (S^-1)	25	62	125	250
	App Viscosity (Pa.s)	6.6	3.8	2.4	1.7

This demonstrated that the apparent viscosity decreased with increasing feed rates, while shear rate increased. Further, the larger nozzle saw tremendously lower shear rates and significantly higher apparent viscosity. From this, it was determined that high deposition rates

could occur using a larger nozzle as apposed to increasing the feed rate. However, this takes away from the level of detail capable of being produced. [28] Figure 27 below highlights the steps this process and shows an example of it in operation.

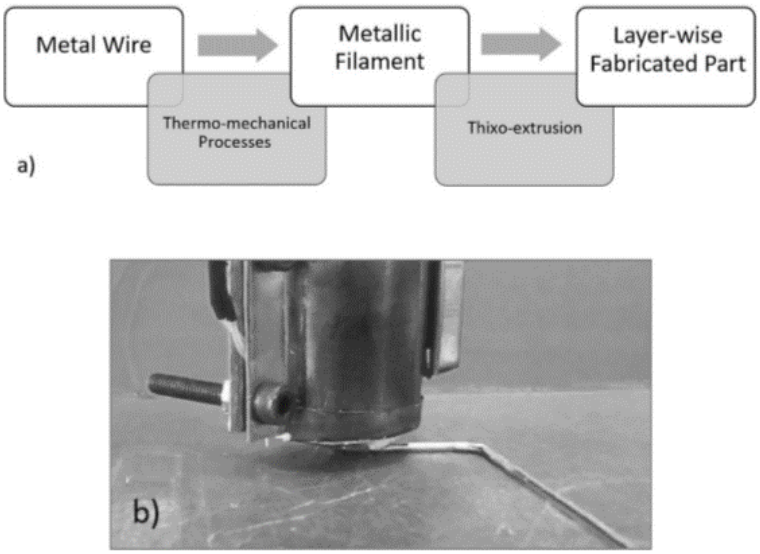

Figure 27: "a) SSMED process graph, b) Single layer depositioning by the process" [28]

CNC Software:

For controlling a CNC gantry, some level of CNC interface or control software is necessary to be implemented. One of the most popular and readily available 3D printer options is Cura. Cura is an open-source software freely available, and designed specifically for the control of three-axis 3D printers. In an effort to develop more economically feasible metal 3D printing technology, Anzalone, et al., worked to modify Cura to be more suitable for this task. [29]

Several machining CNC codes are available as well, such as bCNC, MACH3, and HSM. These could be employed by modeling the print head as a tool, and correcting the offset between passes based on the offset of the deposited bead. Aside from this, there are limited available coding options for metal 3D printers, especially for extrusion based machines. Code for simple geometries

can be written by a user and directly loaded into an interface software. However, for anything more advanced, a modified 3D printer software such as Cura or a modified machining software like the ones listed above would be needed.

Evaluation of Parts:

NIST, the National Institute of Standards and Technology, published a review detailing material properties for parts produced using additive manufacturing methods. This report covers several destructive and deformative tests, such as tension tests, compression tests, bearing tests, modulus tests, and hardness tests. It also reviews failure properties such as fatigue, fracture toughness, and crack growth. [30]

Tension tests consist of uniaxial tensile loading of metals at room temperature for specific test sample geometries. The methods employed are referred to as ASTM E8, which details geometric requirements of the specimens. Figure 28 provides an example of the test speciments for this analysis.

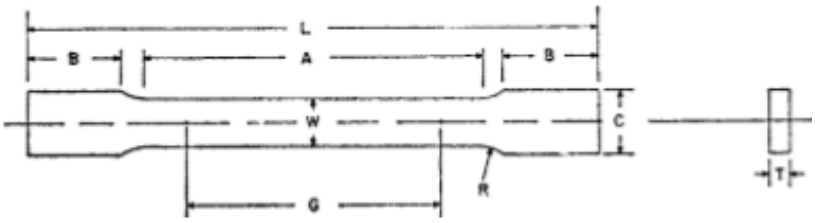

Figure 28: Example of a Standard Tension Test Specimen [31]

Due to the nature of layering and deposition patterns, there can be changes in the material properties throughout the part. “[A]dditional information about construction procedure for the additive manufactured part must be reported. The information reported must include location and

orientation of the part in the additive manufacturing system build volume. This is due to the potential anisotropic behavior of additive manufacturing."[7]

In his Masters' thesis research, Gades pointed out that the process of MIG additive manufacturing could be used to substitute sand casting. [7] Therefore, it is also important to examine potential casting conditions and standards for aluminum parts. Akhyar, et al., worked to analyze the cooling rates, microstructure, and hardness of aluminum casting alloys to give a basis point. This study looked at effects such as alloy composition, temperatures, and the allowed rates of cooling. In it, they found that high silicon contents led to higher hardness in the aluminum alloys. [32]

ASTM International also published standards for aluminum sand casting parts to ensure they met the necessary qualifications. These gave gradings for the casting based on alloy percentage breakdowns, as well as certification and inspection processes used to review individual parts. [33] Figure 29 showcases the steps of the hardness testing process below.

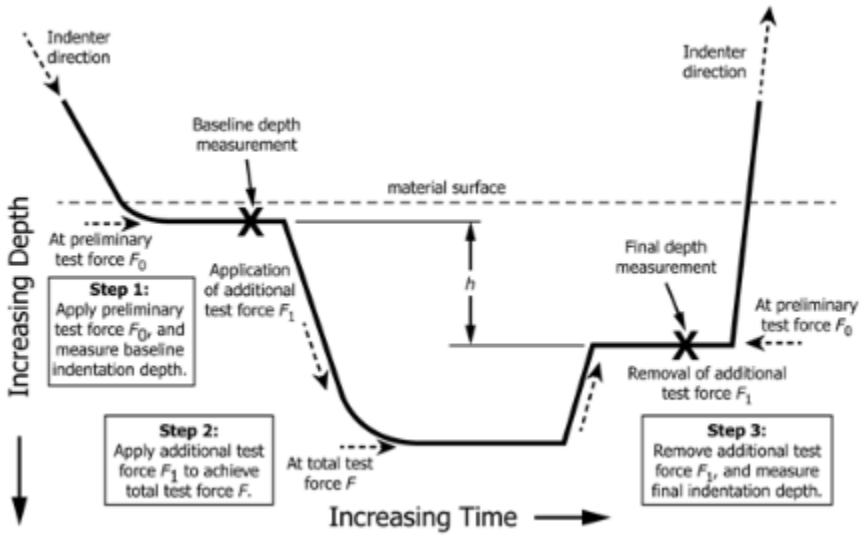

Figure 29: Rockwell Hardness Test Method (Schematic Diagram) [34]

Another method to evaluate parts produced by this method is Rockwell hardness testing. This will allow for consistency to be established in the printed parts. ASTM has published standards and guidelines for hardness testing. These standards cover the conditions for testing including the operation of the test, sample preparation, and other concerns such as temperature. [34] The calibration of these machines is also crucial to its successful operation. Calibration guidelines are included within the full ASTM standards. Furthermore, the standards for operation of the machines based on different materials is provided in these standards, such as the values to set the indention force at and the type of indenter to use. [34] Table 8 provides useful information for the different Rockwell Scales.

Table 8: Rockwell Hardness Scales [34]

Scale Symbol	Indenter	Total Test Force, kgf	Dial Figures	Typical Applications of Scales
B	1/16-in. (1.588-mm) ball	100	red	Copper alloys, soft steels, aluminum alloys, malleable iron, etc.
C	diamond	150	black	Steel, hard cast irons, pearlitic malleable iron, titanium, deep case hardened steel, and other materials harder than B100.
A	diamond	60	black	Cemented carbides, thin steel, and shallow case-hardened steel.
D	diamond	100	black	Thin steel and medium case hardened steel, and pearlitic malleable iron.
E	1/8-in. (3.175-mm) ball	100	red	Cast iron, aluminum and magnesium alloys, bearing metals.
F	1/16-in. (1.588-mm) ball	60	red	Annealed copper alloys, thin soft sheet metals.
G	1/16-in. (1.588-mm) ball	150	red	Malleable irons, copper-nickel-zinc and cupro-nickel alloys. Upper limit G92 to avoid possible flattening of ball.
H	1/8-in. (3.175-mm) ball	60	red	Aluminum, zinc, lead.
K	1/8-in. (3.175-mm) ball	150	red	
L	1/4-in. (6.350-mm) ball	60	red	
M	1/4-in. (6.350-mm) ball	100	red	Bearing metals and other very soft or thin materials. Use smallest ball and heaviest load that does not give anvil effect.
P	1/4-in. (6.350-mm) ball	150	red	
R	1/2-in. (12.70-mm) ball	60	red	
S	1/2-in. (12.70-mm) ball	100	red	
V	1/2-in. (12.70-mm) ball	150	red	

As these samples will be made from aluminum alloys, the scale that will be used is Rockwell hardness B, abbreviated HRB. A tungsten carbide ball indenter is necessary and a test force of 100 kg will be applied. The hardness value assigned on this scale is based on the depth of indention. Using the recorded hardness values, an average hardness and a range of hardness can be determined from the results. These equations define these values, where H represents hardness, R represents the range, and n is the number of samples.

$$\overline{H} = \frac{H_1 + H_2 + \cdots + H_n}{n} \quad (7)$$

$$R = H_{max} - H_{min} \quad (8)$$

Summary of Research Opportunities:

Wire based metal extrusion has already been shown to be a viable form of additive manufacturing. However, limited research has been done into developing it as a fully commercialized technology. Furthermore, this process has seen little to no experimentation in conjunction with induction heating, which could allow for significantly lower power requirements and costs to produce parts. [27, 28]

Casting processes have also shown that methods exist to allow for low cost production of parts on a large scale, or for rapid prototyping of individual parts. By implementing knowledge from the various casting processes explored, developments could be made into improving the part quality of semi-solid extruded parts. [14, 21]

Another novel approach was the introduction of the wire feed to the system. By attempting to fully melt the feedstock in the print head and develop the necessary shear force as extrusion occurs, the complexity and cost of previous thixo-extruding and rheo-extruding processes could be reduced.

Furthermore, there was no clear parameterization of similar wire extrusion methods of additive manufacturing, whether semi-solid or fully molten. This would aid in creating wire based extruded additive manufacturing processes as a viable commercial technology, and would lay the groundwork for future work in this area.

IV: Design of Equipment

Overview:

The design pursued in this research utilized readily available hardware to build a machine capable of producing additive manufactured parts. Initial tests have indicated potential for high resolution, rapid build times, and greatly decreased costs compared to other systems available. Phase I development sought to verify these benefits and improve the prototype design to better achieve them. Figure 30 provides a block diagram overview of the functional design of this prototype.

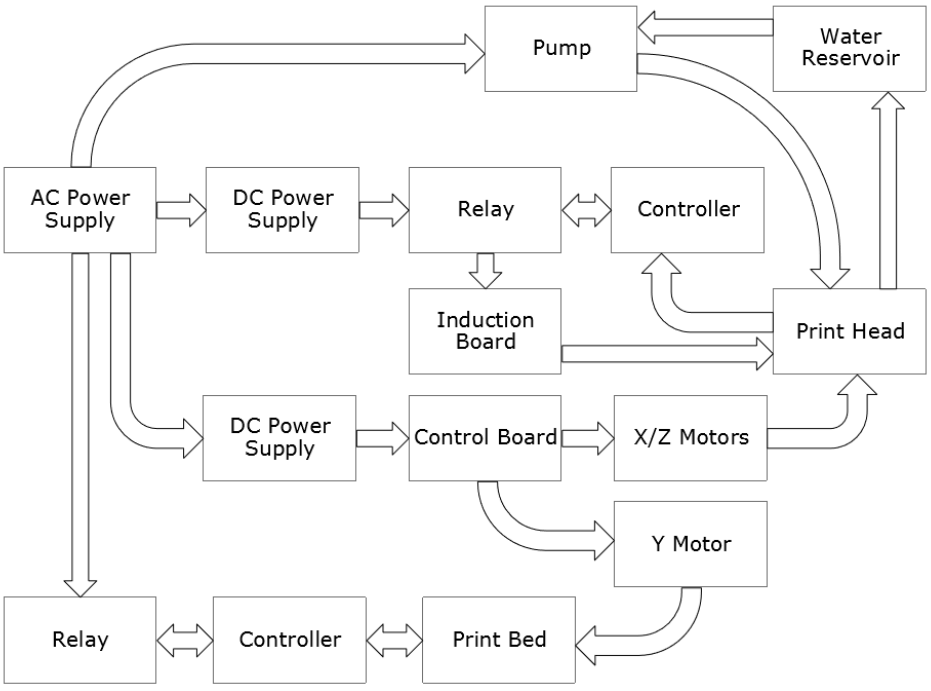

Figure 30: Block Diagram of Printer Prototype

The printing method involved in this technology was the induction heating system used to heat metal to a semi-solid or fully molten state. Induction heating uses electromagnetism to induce eddy currents within magnetic materials. The system that was designed for this technology begins

with a DC power supply that was used to power the induction circuit board with an isolated and regulated voltage. At the induction circuit board, the DC power was converted to AC through power inverters at a controlled frequency. From here, the power was transmitted to a copper coil. Suspended within the copper coil was an electrically conductive crucible/nozzle. The current design involves pre-filling this nozzle with the desired metal to print. The modular design of the print head would allow the user to easily swap the pre-filled nozzle based on the metal desired. The electromagnetic field created by the induction coil creates small eddy currents within the nozzle, which creates heat. In order to limit the heat build-up in the coil itself, a cooling water circuit pumps water through the coil.

Metal fed through an opening located at the top of the nozzle can be heated to high temperatures quickly by this process. Temperature controllers for the nozzle and bed regulated the temperature. It is planned to replace these systems with a dedicated motherboard that will also control the motor board and user interface. The temperature control allowed the metal to be heated to either fully molten or a semi-solid state. Both have been observed in testing; however, more work will be done to determine which state will be better suited for this technology.

The bed was heated using resistive heating elements placed within a steel bed that allows for heat transfer into a build plate above. On this build plate was an aluminum mesh that was fixed in place around the build plate. This mesh was heated to just below the melting point of aluminum, and when the molten material was deposited onto the mesh, the deposited material melted just enough to stick in place.

Currently, the test prototype has been produced for a fraction of the cost of most other systems. The design used readily available hardware to fabricate this machine. The prototype has been tested by loading metal rod, metal wire, and a specially made braided wire into the crucible.

The crucible was made of an electrically conductive material, allowing for the induction coil to rapidly heat it. The metal was melted within the crucible and proceeds out of the bottom of the nozzle onto a build plate by means of extrusion from the incoming metal wire, pultrusion from the adhesion to metal already deposited, and shielding gas flow.

The feed system utilized a spool of the braided wire or off-the-shelf welding wire. A prototype rod fed system has undergone some testing, but would require further development. Two feed gears mounted to a motor grab the incoming metal and feed it into the crucible. This allows for uninterrupted feed so long as the user monitors the amount of feedstock available and added more when necessary.

The feed was also aided by a shielding gas delivery system proprietary to this design. This system delivers shielding gas to the nozzle to provide cooling and prevent negative effects such as oxidation. The gas flow made depositing the metal easier, as well as allowing for greater control of the material flow. The low pressure and fluid flow also created additional pultrusion, which pulls the metal out through the nozzle.

The print head and print bed were attached to ball screws driven by stepper motors. These were used to control movement in the X, Y, and Z axes. Computer control of these motors allowed the print head to be guided along the desired deposition path in order to create the designed part. Either G-code written for a part by a user or by a computer-aided design software could be used by the printer to fabricate the printed part.

The current model, while small in size, is scalable to meet a multitude of applications. At the moment, the main body of the printer is roughly 1’ x 1’ x 2.5’, with a few components positioned off of the main body. These components can be integrated into the frame in future

builds. While much improvement can still take place, this machine has shown great promise while eliminating the issues associated with other additive manufacturing technologies.

Feed System:

In order to aid the direct metal deposition of a wire based additive manufacturing system, a secondary gas-aided feed system was designed and implemented. This system relied on several fluid dynamics principles to encourage constant material extrusion for a fused deposition modeling system, as well as provide cooling and thermal control of the incoming feed material. This was supplementary to the direct material extrusion created by the pressure of the incoming metal feed wire onto the melt pool.

The direct material extrusion was based on creating a constant melt pool within a specially designed crucible/nozzle. This melt pool of material was driven out by the pressure created by incoming non-melted material at the top of the melt pool, creating material extrusion at the bottom of the melt pool through an orifice. As the melt pool was driven out of the nozzle, there was a secondary effect caused by adhesion. When the material adheres to either the print bed or previous layers already deposited, an effect called pultrusion occurs, where material was actively pulled from the melt pool due this adhesion.

This direct metal extrusion/pultrusion process was insufficient to create a reliable deposition process, however. To improve this, a secondary feed system was designed as well. This system used a shielding gas appropriate to the material selected. In the case of aluminum, argon was the gas used, however the gas chosen can vary for steel or other materials.

The first purpose of this gas-aided system was to provide a pressure head at the top of the melt pool to prevent back-flow of the molten material. This was achieved by a 1/16” hole drilled

at a 30°-45° angle into a ceramic guide. A tube to carry and deliver this gas was inserted into this hole so that a downward flow occurs, creating the desired pressure head. This gas tube at the top of the melt pool also cools the incoming material. This material was prone to heat transfer up the length of the wire, and by creating gas flow over the incoming material, it allowed for convective cooling to occur, transferring heat away from the incoming wire. Figure 31 provides a look at the feed system assembly as well as the flow of materials through it.

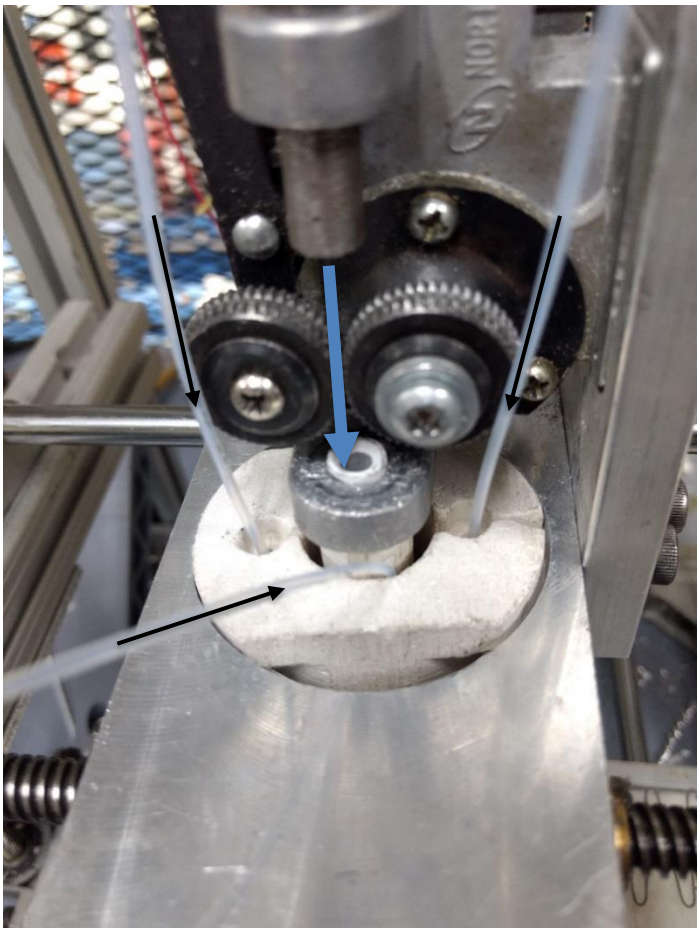

Direction of Argon Flow Within Gas Tubes

Direction of Wire Feed Through Rollers Into Ceramic Guide

Figure 31: Wire Feed with Gas-Aided System

This gas-aided system also flowed over the bottom of the nozzle at the orifice through which the material exits. This was achieved by channels created in an insulative housing surrounding the crucible/nozzle. This channel is a 1/16” hole that runs vertically, then angles to 45° to deliver the gas at this angle over the nozzle orifice. This created what is called the Bernoulli effect, which decreased pressure at the opening of the nozzle. This allowd for the material to flow more readily through the orifice, creating constant material deposition.

Print Head:

In order to extrude material reliably using wire feedstock, a special system was designed and implemented to ensure repeatable operation. This system began with an induction print head design for material extrusion for a fused deposition modeling additive manufacturing system. This was comprised of a unique feed wire design, a melting crucible/nozzle, an insulative support housing for the crucible/nozzle, and a ceramic guide for the feed wire. The entire system was designed to be modular, so that different pieces can be substituted based on the requirements of the operator.

The feed wire was a braided or twisted stock created from 0.047” ER 4043 welding wire. This wire was braided to a target diameter of 0.070”-0.090”. The purpose of the braided wire was to create a feed material that is still flexible and can be spooled, but more rigid than traditional welding wire. The added rigidity prevented bending in the wire that could be found in standard wire feed systems. The braided wire also had a greater surface area than standard cylindrical wire.

This gave a unique advantage over using a cylindrical wire at the same diameter. The greater surface area allows for faster heat transfer, which improves the melt rate of the incoming feed stock. This ties into controlling the melt pool for deposition. The use of this braided feed wire

was unique to this design and allowed many advantages over other methods of wire material extrusion. Figure 32 provides an example of the braided feed wire created for this method.

Figure 32: Example of Braided Wire

This method also allowed for future development with multi-materials, either through the ability to change the spool mid-print to an alternate material, or experimentation with braiding multiple material wires together. Both of these hold great potential for utilization, and were unique to this method of feed style developed as part of this research. However, more work would need to be done separately to explore further into this are.

Figure 33: Prototype Steel Crucible/Nozzle

An early prototype of the crucible and nozzle is shown in Figure 33. The melting crucible and nozzle combination was an electrically conductive cylinder at 3/8” outer diameter with a 3/16” inner diameter. At the top of the cylinder was a ¾” diameter disc to hold the nozzle in the insulative housing. The length of the nozzle can vary depending on the application of the printer set up. At the lower end of the cylinder is a 45 degree angle cone, ending in an orifice for material deposition. This orifice can vary greatly in diameter as well, depending on the size of material layers desired. The modular design allowed for this nozzle to be easily removed and replaced with different lengths and diameters for different circumstances. This modular design was a unique innovation allowing one machine to be customized to fit several needs of users.

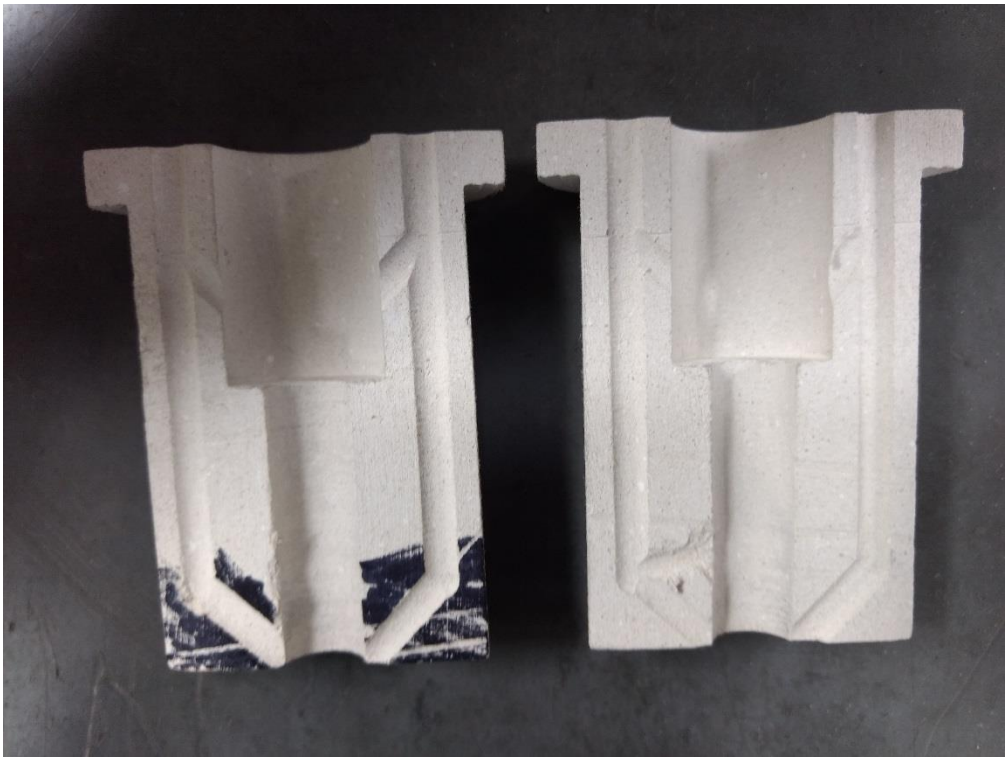

Figure 34: Prototype Insulative Housing

The insulative housing for the crucible was made from an inorganic ceramic consisting of lime, silica, and reinforcing fibers. Figure 34 above shows the design of the initial insulative housing. In this case, the brand SuperFireTemp has been used for the housing. This rested in an aluminum bracket connected to the frame and drive system of the printer. The interior of the housing matched the dimensions of the nozzle to suspend the nozzle within the induction coil. The housing also decreased heat transfer from the crucible/nozzle to the rest of the printer. By suspending the nozzle, it can easily be interchanged for other nozzle sizes to fit various applications. Further, the housing was suspended freely in the aluminum bracket, so that it too can be easily swapped with other insulative housings to fit different nozzles.

The ceramic guide tube was designed to help control the path of the braided wire into the crucible/nozzle. This guide was made from alumina bisque, though other ceramics could be

utilized. A traditional welding spool gun feed system is used to move the wire. After this, it enters a ceramic guide, which prevents misalignment from the feed system to the crucible/nozzle. Further, the guide extended into the crucible/nozzle to control the volume of the melt pool. This was typically one-third of the length of the nozzle, which makes the melt pool two-thirds height of the 3/16” inner diameter, which varies based on the set up. Figure 35 shows the first prototype ceramic guide tube used in this experiment.

Figure 35: Prototype Ceramic Guide Tube

Induction Circuit:

The heating method for this printer was based around an induction circuit surrounding the nozzle. This induction circuit was designed for the carbon steel nozzle/crucible that was created for the printer. In this setup, the induction coil operated at 95 kHz and 20 amperes. A 36 Volt 500

Watt power supply was connected both to a temperature control circuit, discussed later, and a manual switch to turn on and off heating of the print head by an operator.

The initial design was performed experimentally. Using standard measurement diameter feed stock, such as 0.25 inches, 0.5 inches, and 0.75 inches, recordings were taken of the temperature and time to reach steady state of different samples. Ultimately, 0.5 inches was set as the crucible diameter for simplicity of this experiment. Equation 3 can be used to calculate the magnetic field intensity. The coil had 7 turns, operates at 20 amperes, and has a length of 3.6 centimeters.

$$H = \frac{NI}{l}$$

$$H = \frac{7 * 20amps}{3.6cm}$$

$$H = \frac{140amps}{3.6cm}$$

$$H = 39.3\frac{amps}{cm}$$

This can be combined with Table 3, given that the workpiece being heated is carbon steel. Given that the operating frequency is close to 100 kHz, and the magnetic field intensity is roughly 40 amps/cm, then the penetration depth in this particular application can be estimated to be 0.12 cm or 0.005 inches.

By measuring the max temperature of the workpiece during testing, axial magnetic field can be calculated as well using Equation 4, given the same values for *N*, *I*, and *l* as before, and knowing that the magnetic permeability of carbon steel is equal to 1.25 x 10^{-4} H/m.

$$B_z = \frac{\mu_0 NI}{2l}$$

$$B_z = \frac{1.26x10^{-4} H/m * 7 * 20\ amps}{2 * 0.036m}$$

$$B_z = \frac{0.018 \frac{(H * amps)}{m}}{0.072m}$$

$$B_z = 0.245\ \frac{H * amps}{m^2}$$

The last value of note here was work piece power, given by Equation 5. Using the finalized design of the crucible discussed further in this paper, a carbon steel jacket around a stainless steel core was used. The outer diameter of the carbon steel was the same outer diameter as the solid carbon steel core, and little to no changes to the magnetic properties were witnessed or found based on the important values for calculation. This jacket was weighed on a scale and found to have a mass of 13.76g or 0.01376kg. Further, the maximum temperature of the crucible was measured using a K-type thermocouple after the system reached a constant steady state. The time to reach this steady state was about 240 seconds, and the maximum temperature recorded within the induction coil was around 1600°F or 870°C, after being heated from room temperature to begin. The specific heat for carbon steel is 0.466 J/g°C, giving all the needed information to calculate the workpiece power.

$$P_w = mc \frac{T_f - T_{in}}{t}$$

$$P_w = 13.76\ g * 0.466 \frac{J}{g°C} \frac{870°C - 20°C}{240\ sec}$$

$$P_w = 6.41 \frac{J}{°C} * \frac{850°C}{240\ sec}$$

$$P_w = 22.7\ Watts$$

Print Bed:

A print bed optimized for extrusion based additive manufacturing systems or Fused Deposition Modeling Machines was designed for this research . This print bed consisted of a base attached to a CNC gantry, an insulated layer between the base and the heating level, a heating level comprised of cartridge heaters and a heating block that they are secured inside, a 0.25 inch thick build plate of a material with good thermal conductivity and capability to withstanding the temperatures needed for the material being printed, and a mesh overlay of a the same material or adequately similar material to the material being printed.

This system was used to heat the print bed just below the melting point of the material desired to be printed. The actual numerical values differ based on the feed material to be deposited, though the design and methodology remain the same. By heating the print bed just below the melting point, the print bed stays solid and does not degrade. When the metal was deposited onto the heated mesh, the heat of the incoming material allows for the mesh to lightly melt and adhere to the deposited material. This has shown superiority over a solid similar material build plate or a thin foil or film of a similar material overlaid on a build plate in a number of ways:

- Better integrity of the bed, as the foil or solid material often begins to degrade and melt in order to maintain the needed heat throughout
- Better adhesion, as less heat is taken from the deposited material due to the decreased surface area of the build plate

- Easier removal of the build after the print, due to lower surface area contact between the bed and the build from the mesh layout opposed to a solid material
- Lower energy requirements to maintain temperature of the bed

The system currently designed allowed for only partial adhesion between the bed and the part being built at the interface locations between the part and the mesh. This partial adhesion promoted the benefits listed above and helps maintain geometrical accuracy of the print. The exact area of contact between the mesh and the part was dependent on resolution and deposition. The diameter nozzle installed for the desired print changed the level of contact with the mesh. The thickness of the mesh can be changed as well to better match the material deposition thickness. Current testing have shown optimal results with a percentage contact in the range of 35% to 50% of the build area. This requires further testing to refine and confirm.

To encourage the properties and characteristics that were demonstrated, heating the bed to 70%-90% of the melt temperature of the material being deposited has yielded the best results for aluminum. Testing of other materials has yet to take place, and as such values have not yet been confirmed for other materials. Other factors, such as travel rate and material feed rate, are still being set, but preliminary values have been set. The current thickness of the mesh is 0.032 inches. This has been the best tested so far, though there is still room for improvement. Figures 36 and 37 provide examples of this mesh design prior to installation on the machine.

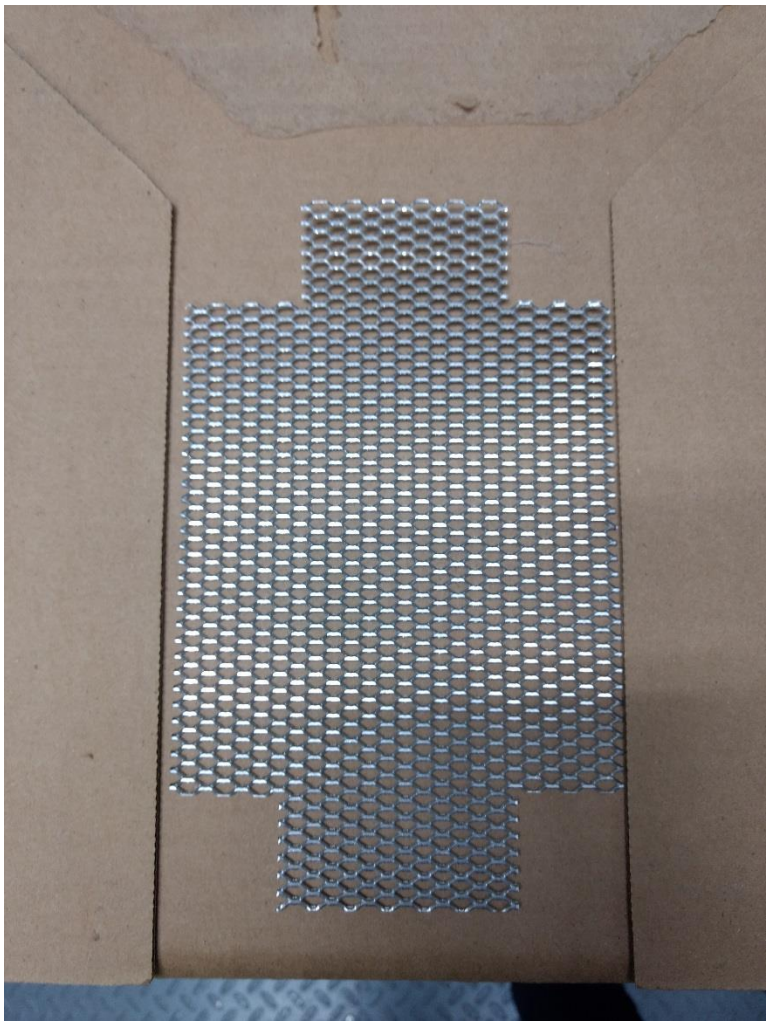

Figure 36: Early Version of Mesh Overlay Prior to Installation

The mesh was mounted to the bed simply by cutting the mesh to roughly 0.5 inches longer than the build area on each side, with 90 degree notches cut out at the corners to allow for folding. The extra length of mesh was then folded around the build plate using a flat surface jig and bent to be tight, starting with one side, then going to the opposite, then repeating for the remaining two sides. After this, the material was pressed flat onto the top, and any adjustments are made to ensure it is a tight fit. This simple method has shown to be effective in securing the material to the bed during printing.

Over time, the material may experience degradation, though typically it is semi-permanent and can last through multiple tests. To date, major wear and degradation has only been seen when melting temperatures were exceeded or damage occurred. This design allows the print bed layer to be removed, the damaged mesh discarded, and a new layer applied when needed, allowing for a more user friendly design and ease of use.

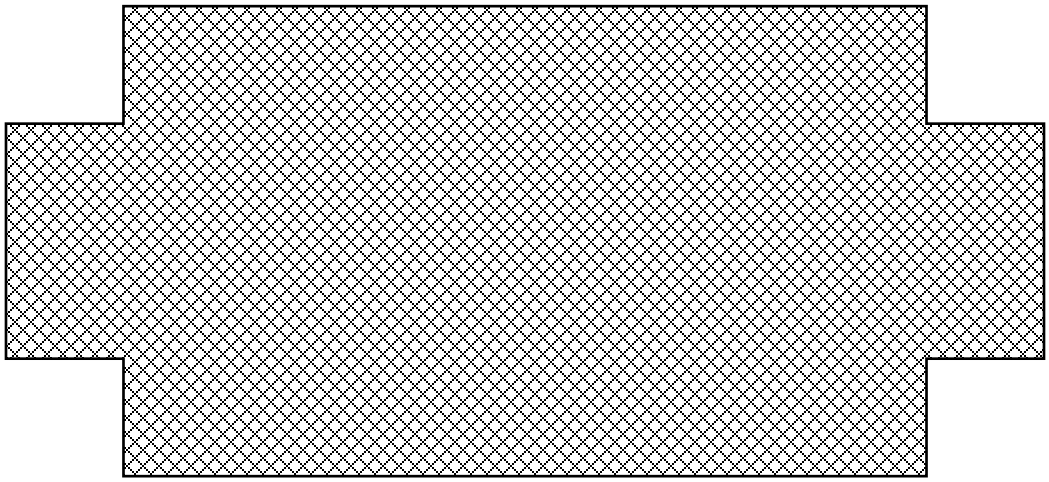

Figure 37: Example of Cut Mesh Sheet Before Installation

Software and Controls:

Open source software has been utilized for the G-Code operation of this printer. In this case, a control board modeled after Arduino and designed for CNC machining uses known as Woodpecker was installed. This board is designed to run with GRBL, an open-source G-Code interface available online. GRBL allows for a wide degree of customization for machine design, and has been adapted to work for additive manufacturing rather than subtractive manufacturing. The G-Code programs for this machine have been written either completely by the user or through

a custom made Python code generator designed for this machine developed by Travis Thompson specifically for this research.

For temperature controls on the bed and print head, two proportional-integral-derivative controllers were installed in individual circuits with thermocouples monitoring the points of interest. These PID controllers were wired into solid state relays to control the power going to each heating system so as to ensure the correct temperature was being maintained. This allowed for easy alterations to the temperature set point as well as real-time feedback to adjust accordingly.

Frame and Motion:

The frame of the printer was constructed from 80/20 aluminum bars, with cross-beams added for support as well as mounting points for the other subsystems. The drive systems for all three axes were supported by the aluminum frame. The print head was designed to move in both the x and z axes, with the print bed moving in the y-axis.

The motion systems for these axis consisted of Nema 17 motors driving the x and y axes, and a Nema 23 motor driving the z-axis. The x and y axes motors were directly coupled to ball screw rods, which in turn travel through threaded nuts attached to these axis. The x-axis runs directly through the print head block, while the y-axis is affixed to the bottom of the print bed. The z-axis is connected to a timing belt that connects two separate ball screws. These are attached to either end of the x-axis, allowing the x-axis to lift the x-axis and print head together. Figure 38 shows the finalized frame and assembly of the motion system for this experiment.

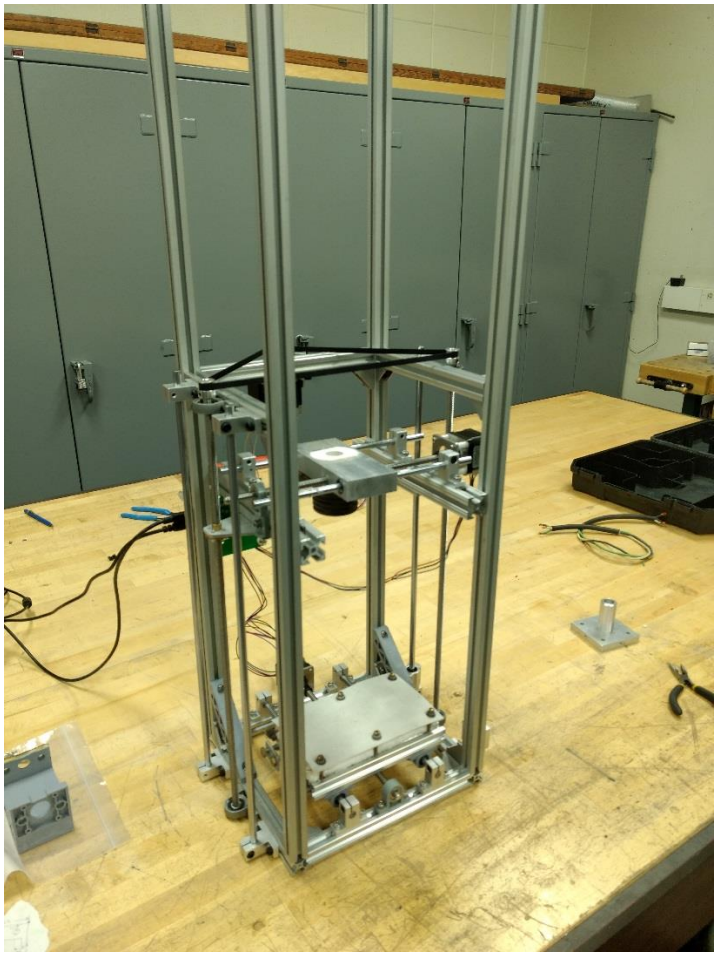

Figure 38: Current Frame Assembly of the Machine

All of these motors were directly wired into the control board mounted on the back of the machine, and controlled via GRBL as discussed previously. This design is easily scalable based on the desired build volume.

Finalized Design:

During the initial testing, discussed below, to parameterize the machine and establish geometrical accuracy, several updates were made to the test model to improve viability and ease of testing going forward. The areas which most notably needed design alterations included the motor feed system, the crucible design, and the feed alignment design. In order to improve the

quality of the material, the accuracy of the print, and the consistency of feed without jamming, these sections were analyzed and design improvements were implemented. Several iterations were tested and implemented to overcome issues discovered during these early tests.

The feed system originally implemented was wire spool gun feed system meant for metal inert gas welding. This system was comprised of a 12 volt DC motor and a set of gears spring-loaded to grip and feed the wire. While this system was able to feed the wire into the print head, it had several issues that prevented it from operating consistently enough for further data collection. These issues included lack of rigidity, misalignment of the feed path, and motor drive issues. This feed system was worn at the time of its installation on the printer, and consequently, it was found the gears could shift slightly causing difficulty in gripping the wire, or allowing misalignment. Further, the coupling between the motor and the feed gears was not rigidly fixed, and the mounting for the entire system caused it to shift slightly away from the needed feed path of the wire allowing the wire to bind or catch. This feed system was mounted to the side and back of the feed system, and had to be aligned manually every time this system was removed and reinstalled to perform maintenance. Due to this, the feed could often jam or bind as the printer was in operation.

The new system was a repurposed feed system from a plastic fused deposition modelling printer. This feed system uses a stepper motor rather than a DC motor. The motor is connected to a gear on the spindle, which is coupled with a larger gear that turns the actual feed system. This stepper motor provided greater torque as well as the ability to microstep the motor to change the range of operation with more ease. Furthermore, the new feed system was more rigid and allowed for better and more consistent contact with the feed wire. Lastly, this system was mounted on either side of the print head, and no longer required manual alignment when it is installed on the machine.

The print head nozzle and crucible underwent a redesign as well. The design at the beginning of testing was a carbon steel crucible with an off the shelf stainless steel 3D printer nozzle. This stainless steel nozzle was found to degrade rapidly in early testing. These nozzles would experience erosion of the orifice, causing the bead thickness to grow over time with usage of the machine. Prior to the parameterization prints, this nozzle was changed to an off-the-shelf tungsten allow 3D printer nozzle. The carbon steel crucible also experienced problems with oxidation, creating impurities in the aluminum.

The crucible material was changed to stainless steel as issues with oxidation forming on carbon steel inside the crucible became apparent. Due to the lower interaction with induction heating possessed by stainless steel, the geometry of the crucible was changed to an I-shaped cylinder. A carbon steel jacket was placed around this cylinder, effectively creating the same diameter with which the induction coil interacted. This allowed for rapid heating using carbon steel without the potential oxidation and debris previously witnessed with this material. The new tungsten nozzle was able to withstand the erosion the previous stainless steel nozzle underwent as well, allowing for greater consistency of deposition between tests. From this point, the geometry of the print was only influenced by the test variables set during parameterization.

In order to determine the amount of heat transfer from the jacket into the stainless steel core, conductive heat transfer could be estimated using the recorded values from testing the heating of the jacket and crucible assembly. The conduction equation is listed below

$$q = \frac{k}{s} * A * \frac{\Delta T}{t} \tag{9}$$

where q is the energy transfer with respect to time, k is the thermal conductivity, s is the thickness of material, A is the cross-sectional area, and ΔT is the temperature differential. The material is a hollow tube of stainless steel with a wall thickness of 0.125 inches or 0.3175 cm. The area is the inner diameter of the carbon jacket, which has a diameter of 0.375 inches or 0.9525 cm and a height of 1.25 inches or 3.175 cm.

$$A = 2\pi \frac{D}{2} h \tag{10}$$

$$A = 2\pi \frac{0.9525}{2} 3.175$$

$$A = 9.5\ cm^2$$

This area was then used to calculate the heat transfer from the carbon steel jacket. While thermal conductivity is a function of temperature and varies, this analysis is at a near steady-state temperature of the outer jacket, supplying constant energy from the induction coil to keep the temperature constant. Due to this, we can hold thermal conductivity as roughly constant over the course of the print in order to get a rough estimate. This value can be estimated to be around 15 W/mK. Using this with Equation 9 allows for this value to be found.

$$q = \frac{15 \frac{W}{mK}}{0.003175m} * 0.00095m^2 * \frac{(1143.15 - 293.15)K}{240\ sec}$$

$$q = 17.3\ J$$

This gave a rough idea as to the heat transfer taking place in the print head. A more precise model could be constructed in future research by not looking solely at steady state conditions as was done here.

The feed control circuit was also moved to a separate circuit specifically to control this stepper motor. While the tests for geometric parameterization were conducted using the spindle motor and the onboard controls for feed, the issues identified during those tests required a redesign to this system. The control software GRBL that was used in development of this machine did not have the ability to implement a stepper motor as the feed mechanism, which required the independent circuit. This feed circuit was designed and assembled by Zane Oligee for a separate project, but was no longer in use. With his help, it was repurposed and installed as the upgraded feed mechanism for this printer. This circuit was comprised of a variable voltage power supply connected to an Arduino with a motor driver wired into it. This motor driver went to a potentiometer that was manually adjusted to change the speed of the new motor. By changing the pin connections on the driver, the motor was able to be microstepped to change the speed ranges available.

In order to control the volumetric flow rate of aluminum into the nozzle, calculations on the stepper motor's operation were performed to determine the feed rate of material. The default step angle of the stepper motor used as for the feed system is 1.8° per step. With the option of microstepping the motor, the best step angle was determined to be half-stepped, or 0.9° per step. With this in mind, the steps per revolution can be expressed as

$$\frac{Steps}{revolution} = \frac{360°}{0.9°} = 400 \tag{11}$$

The feed roller for the system is 0.375 inches in diameter or 0.9525 centimeters. This can be used to determine the feed volume of material per rotation of the feed wheel, assuming perfect contact between the wire and the feed wheel with no slipping. Given that the wire diameter of the feed material is 0.047 inches, or 0.119 centimeters, an estimation of the feed rate can be made.

Typically, the braided wire diameter equals about 0.090 inches, which is close to double the single wire diameter. The braided wire does not take up the same volume as a cylinder with this diameter, but the cross-sectional area of the braided wire is equal to double the cross-sectional area of a single wire. This can be used to calculate the volume of wire fed per rotation of the feed roller.

$$V = 2A * C \tag{12}$$

where *A* is the cross-sectional area of a single wire and *C* is the circumference of the feed roller. The circumference of the feed roller is equal to

$$C = 2\pi r = 2\pi * \frac{0.9525}{2} = 2.99\ cm \tag{13}$$

Putting these values in gives

$$V = 2 * 0.0069 cm^2 * 2.99\ cm$$

$$V = 0.041\ cm^3$$

So, the machine fed 0.041 cubic centimeters of material per rotation of the feed roller. The step rate of the feed motor was be varied experimentally to determine a proper range for feeding. Lastly, multiplying the volume by the density of the material gave us the mass flow into the crucible per rotation. Given that the density of aluminum is 2.7 g/cm^3,

$$m = V * \rho = 0.041 cm^3 * 2.7 \frac{g}{cm^3} = 0.1107\ g \tag{14}$$

Due to the complexity of solving the heat generation equation for induction, a simulation was created instead to estimate the temperature distribution of the crucible designed for this application. This was done in SolidWorks using experimental temperature data collected on the machine, as well as the predictive analysis the thermal study created. Radiative, convective, and

appropriate conductive heat transfers were applied to the model, and the simulation was run to determine what the temperature at the lower part of the crucible would be. The heat generation from induction was focused in the carbon steel jacket, simulated in this model. As the nozzle is at the lower end, this model gives an idea as to the temperature at the deposition point of the material. Figure 39 shows the results of this thermal study.

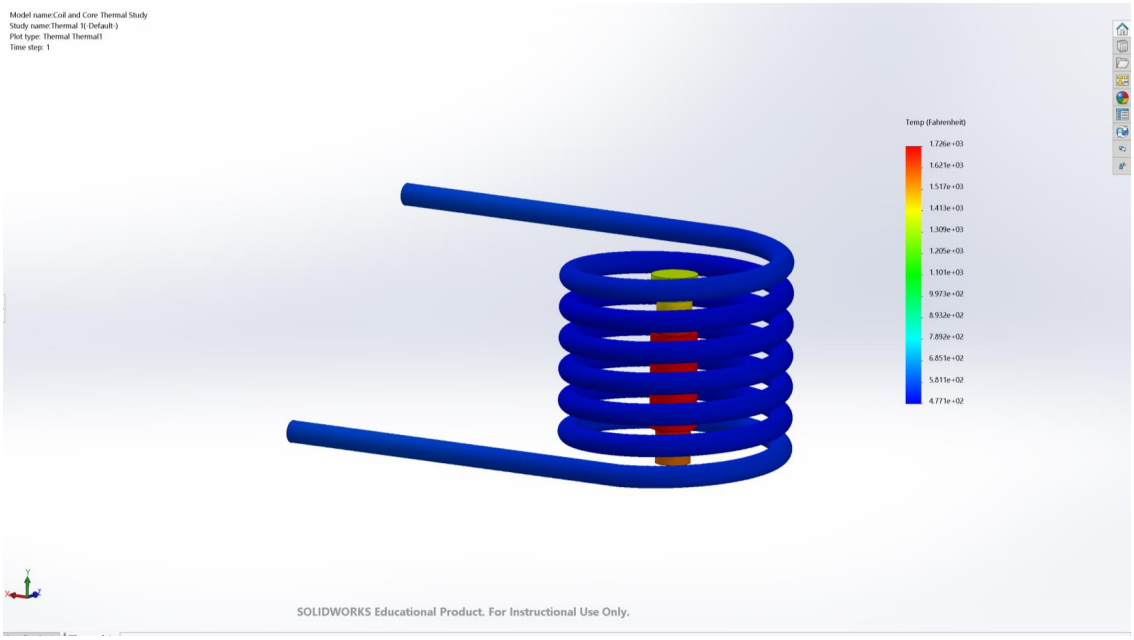

Figure 39: Results from Thermal Study

This image is included in Appendix D in a larger size so that it is more legible. The temperature at the base of the crucible appears to be around 1400° F to 1500°F. While the nozzle will extend slightly lower, this give an idea of the temperature range here, and shows that it was sufficient for melting the feed aluminum still, given that the melting point is around 1100°F.

V: Methodology

The initial goal during the development was to qualify the ability of the method and prototype machine developed as part of this research to produce parts in accordance with a user's specifications. As such, several factors need to be considered to determine if the part produced meets the needs of its designer. One major aspect of this is the geometrical accuracy of the part, or, whether or not the dimensions of the printed part match the dimensions of the model. This area is the primary concern at this stage of development. Other factors of concern for the part include the strength of the part produced, which can be determined both by the strength of the metal deposited as well was the adhesion between layers, and the grain structure of the material.

Important variables of the machine itself to be determined include the speed at which material is fed into the nozzle, the temperature of the nozzle, the temperature of the bed, the travel rate of the print head, and the flow rate of argon into the print head. These variables were identified as the main focus of this study, and by changing the values, different results were produced in the printed parts. Two different goals were set to be achieved through variation of these variables: the quality of parts created using this method, and the optimal initial settings for the operation of this machine. While the goal was not to conduct a complete parameterization of this method, it was desired to find baseline operating conditions that allowed the machine to perform consistently while maintaining good results.

The geometry of the print was a two-dimensional print traveling in the x and y direction in alternating orders. This produced a box-step shape that could test the consistency of the print with regard to the desired shape. This pattern was selected in order to try to allow consistent cooling

and prevent issues that could be seen in typical casting applications. The goal of this shape is to resist potential cracking or stress formations based on cast geometry.

To analyze geometrical accuracy, code to print a desired shape was created. This code varied based on each test, but during each individual test set dimensions were determined for the print. A variable was altered each test in response to issues seen in the previous test, while holding the other variables constant. In order to determine the accuracy of the machine, the print produced was measured and compared to the values entered into the code for the dimensions of the object. After each print, the variable set values were recorded and the print allowed to run. After this, the parts were measured in the x-dimension, y-dimension, and the thickness of the bead using a pair of dial calipers. The percent error between the set dimensions and the actual dimensions was determined. As the parameters were varied, this percent error was sought to be decreased.

Thirty tests were run in total to establish data trends with variation of feed rate, argon flow, and travel rate of the printer. In initial testing, both print head temperature and print bed temperature were found to have little impact on theses tests, and for the sake of reducing the number of variables, were held constant during these runs. The external nozzle temperature was controlled at 1200°F and the print bed was controlled at 800°F. These were held constant both to eliminate variables in order to focus on the feed rate, argon flow, and travel rate to determine what effect changes in these values had on the final product.

Originally, it was intended to begin gathering data on the material properties of the aluminum parts printed by this new method of additive manufacturing. Unfortunately, issues with blockages forming in nozzle began to occur. This led to jamming and difficulty producing the tests for material properties data. Several solutions are underway at the time of writing this to determine and eliminate these blockages, but were unable to be implemented in a timely manner for this

research. Nonetheless, code, strategies, and planning for how to obtain this data was drafted as part of the methodology for this thesis. This was built around the printing of 3D hollow boxes in order to take the walls and perform destructive testing to gather data comparable to stock aluminum samples. These methods could easily be implemented into future research for ongoing development and validation of this method of additive manufacturing.

Hardness tests were performed on samples produced through direct extrusion on to the print bed. These were small samples made simply by layering material at one location and allowing them to freeze. These samples were of roughly the same size and shape, around 0.5 inches to 0.75 inches in diameter. The samples were allowed to cool and freeze over 3 to 6 seconds. These samples would be analyzed using Rockwell Hardness Scale B (HRB) tests to determine the consistency of the print.

VI: Results

The 30 tests conducted were based on the two-dimensional geometry discussed above. These the geometrical accuracy based on percent error in the x and y dimension and the bead thickness were recorded for each. The quality of these prints varied and overall improved with each successive test. The percent error is calculated using

$$Percent\ Error = \frac{|x_{measured} - x_{theoretical}|}{x_{theoretical}} \tag{15}$$

This was recorded for each dimension of each test, and then compiled into an average percent error for each test. The full recorded data set for this test can be found in Appendix B of this thesis. Figure 40 below shows the final product of each test print run.

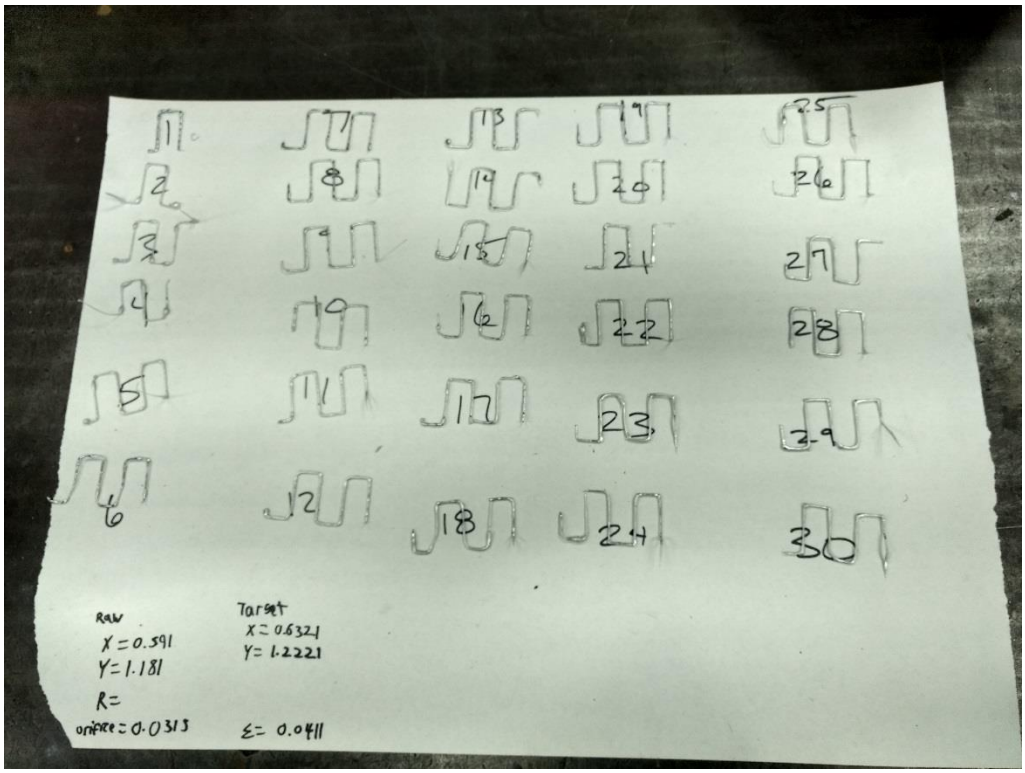

Figure 40: Box-Step Test Samples

The average percent error for the x dimension was 1.23%, the average percent error for the y dimension was 1.78% and the average percent error for the bead thickness was 8.6%. This was using a target x dimension of 0.632 inches, a target y dimension of 1.221 inches, and a target bead thickness of 0.044 inches.

Hardness test samples were produced as well to evaluate machine consistency and material properties. Figure 41 below shows the printed samples used for these hardness tests. Five samples were produced, with each sample having three hardness tests performed on the surface.

Figure 41: Hardness Testing Samples

These samples were tested from left to right in order to track which location gave which measurement. Table 9 below contains the results of each hardness test performed. This was done using a Rockwell Hardness Tester located in Wilmore Laboratories. This machine undergoes regular calibration by the staff at Wilmore to ensure accuracy. Rockwell hardness scale B (HRB) was used for this material.

Table 9: Hardness Testing Data of Aluminum Samples

Sample Number:	Test Number:	Hardness (HRB):
1	1	67.9
1	2	79.2
1	3	87
2	1	71.2
2	2	71.5
2	3	83
3	1	73.4
3	2	81.6
3	3	86.1
4	1	69.8
4	2	89.4
4	3	87
5	1	69.4
5	2	80.7
5	3	79.3

Using Equations 7 and 8, the average hardness and hardness range can be determined. This helped in evaluating the consistency of the parts produced.

$$\bar{H} = \frac{67.9 + 79.2 + \cdots + 79.3}{15}$$

$$R = 89.4 - 67.9$$

$$\bar{H} = 78.4\ HRB$$

$$R = 21.5\ HRB$$

From this, it can be seen the tests span a range of 21.5 HRB and have an average hardness of 78.4 HRB.

VII: Discussion

Statistical analysis could be performed on this data in order to determine meaningful information regarding the performance of this method of metal additive manufacturing. The data from the geometrical box-step tests could be utilized to determine which variables were impactful on the final quality of the print geometry in adhering to the desired specifications. There are a variety of tools that can perform this analysis. For these tests, linear regression was implemented using Microsoft Excel on the data obtained. This was performed for each input variable, argon flow, feed rate *S*, and travel speed *F*, with regards to each measured error, the x-dimension error, the y-dimension error, and the bead thickness error.

The values of most interest within this analysis were the coefficient of correlation, *R*, the significance *F* value, and the *P*-value. These can all indicate whether or not there was strong correlation between the independent and dependent variables. Table 10 through Table 18 provide regression results for each independent variable with regard to each dependent variable.

Table 10: Regression of Argon with Regard to X Error

SUMMARY OUTPUT

Regression Statistics	
Multiple R	0.2253752
R Square	0.050793981
Adjusted R Square	0.016893766
Standard Error	0.01629994
Observations	30

ANOVA

	df	*SS*	*MS*	*F*	*Significance F*
Regression	1	0.00039809	0.00039809	1.498338018	0.23112758
Residual	28	0.007439265	0.000265688		
Total	29	0.007837356			

	Coefficients	*Standard Error*	*t Stat*	*P-value*	*Lower 95%*	*Upper 95%*	*Lower 95.0%*	*Upper 95.0%*
Intercept	-0.035606459	0.039273974	-0.906617159	0.372345747	-0.116055548	0.04484263	-0.116055548	0.04484263
Argon	0.001972664	0.001611566	1.224066182	0.23112758	-0.00132848	0.005273808	-0.00132848	0.005273808

Table 11: Regression of Feed Rate *S* with Regard to X Error

SUMMARY OUTPUT

Regression Statistics	
Multiple R	0.076600809
R Square	0.005867684
Adjusted R Square	-0.029637042
Standard Error	0.016681222
Observations	30

ANOVA

	df	*SS*	*MS*	*F*	*Significance F*
Regression	1	4.59871E-05	4.59871E-05	0.165264871	0.68744546
Residual	28	0.007791369	0.000278263		
Total	29	0.007837356			

	Coefficients	*Standard Error*	*t Stat*	*P-value*	*Lower 95%*	*Upper 95%*	*Lower 95.0%*	*Upper 95.0%*
Intercept	-0.001038858	0.033024413	-0.031457275	0.975128031	-0.068686301	0.066608585	-0.068686301	0.066608585
S	5.2527E-05	0.000129209	0.406527823	0.68744546	-0.000212146	0.0003172	-0.000212146	0.0003172

Table 12: Regression of Travel Rate *F* with Regard to X Error

SUMMARY OUTPUT

Regression Statistics	
Multiple R	0.056476594
R Square	0.003189606
Adjusted R Square	-0.032410766
Standard Error	0.016703675
Observations	30

ANOVA

	df	*SS*	*MS*	*F*	*Significance F*
Regression	1	2.49981E-05	2.49981E-05	0.08959473	0.76690361
Residual	28	0.007812358	0.000279013		
Total	29	0.007837356			

	Coefficients	*Standard Error*	*t Stat*	*P-value*	*Lower 95%*	*Upper 95%*	*Lower 95.0%*	*Upper 95.0%*
Intercept	0.016494623	0.014246115	1.157833082	0.256713475	-0.01268722	0.045676466	-0.01268722	0.045676466
F	-8.11432E-06	2.71088E-05	-0.299323787	0.76690361	-6.36442E-05	4.74156E-05	-6.36442E-05	4.74156E-05

Table 13: Regression of Argon with Regard to Y Error

SUMMARY OUTPUT

Regression Statistics	
Multiple R	0.15135533
R Square	0.022908436
Adjusted R Square	-0.011987691
Standard Error	0.012551095
Observations	30

ANOVA

	df	*SS*	*MS*	*F*	*Significance F*
Regression	1	0.000103414	0.000103414	0.65647502	0.42464017
Residual	28	0.00441084	0.00015753		
Total	29	0.004514254			

	Coefficients	*Standard Error*	*t Stat*	*P-value*	*Lower 95%*	*Upper 95%*	*Lower 95.0%*	*Upper 95.0%*
Intercept	-0.006648412	0.0302413	-0.219845445	0.827586477	-0.068594907	0.055298083	-0.068594907	0.055298083
Argon	0.001005432	0.00124092	0.810231461	0.42464017	-0.001536477	0.003547342	-0.001536477	0.003547342

Table 14: Regression of Feed Rate *S* with Regard to Y Error

SUMMARY OUTPUT

Regression Statistics	
Multiple R	0.077683472
R Square	0.006034722
Adjusted R Square	-0.029464038
Standard Error	0.012659006
Observations	30

ANOVA

	df	*SS*	*MS*	*F*	*Significance F*
Regression	1	2.72423E-05	2.72423E-05	0.169998104	0.683253306
Residual	28	0.004487012	0.00016025		
Total	29	0.004514254			

	Coefficients	*Standard Error*	*t Stat*	*P-value*	*Lower 95%*	*Upper 95%*	*Lower 95.0%*	*Upper 95.0%*
Intercept	0.028072621	0.025061487	1.120149836	0.272166446	-0.023263508	0.07940875	-0.023263508	0.07940875
S	-4.04284E-05	9.80538E-05	-0.412308263	0.683253306	-0.000241282	0.000160426	-0.000241282	0.000160426

Table 15: Regression of Travel Rate *F* with Regard to Y Error

SUMMARY OUTPUT

Regression Statistics	
Multiple R	0.071615547
R Square	0.005128787
Adjusted R Square	-0.030402328
Standard Error	0.012664773
Observations	30

ANOVA

	df	*SS*	*MS*	*F*	*Significance F*
Regression	1	2.31526E-05	2.31526E-05	0.144346345	0.706864491
Residual	28	0.004491101	0.000160396		
Total	29	0.004514254			

	Coefficients	*Standard Error*	*t Stat*	*P-value*	*Lower 95%*	*Upper 95%*	*Lower 95.0%*	*Upper 95.0%*
Intercept	0.02179225	0.010801444	2.017531242	0.053316916	-0.000333504	0.043918005	-0.000333504	0.043918005
F	-7.80907E-06	2.0554E-05	-0.379929395	0.706864491	-4.9912E-05	3.42939E-05	-4.9912E-05	3.42939E-05

Table 16: Regression of Argon with Regard to Bead Thickness Error

SUMMARY OUTPUT

Regression Statistics	
Multiple R	0.096458894
R Square	0.009304318
Adjusted R Square	-0.02607767
Standard Error	0.077120709
Observations	30

ANOVA

	df	*SS*	*MS*	*F*	*Significance F*
Regression	1	0.001564027	0.001564027	0.262967646	0.612110794
Residual	28	0.166532907	0.005947604		
Total	29	0.168096934			

	Coefficients	*Standard Error*	*t Stat*	*P-value*	*Lower 95%*	*Upper 95%*	*Lower 95.0%*	*Upper 95.0%*
Intercept	0.181230202	0.18581889	0.975305587	0.337760123	-0.19940254	0.561862943	-0.19940254	0.561862943
Argon	-0.003910068	0.007624883	-0.512803711	0.612110794	-0.019528934	0.011708797	-0.019528934	0.011708797

Table 17: Regression of Feed Rate *S* with Regard to Bead Thickness

SUMMARY OUTPUT

Regression Statistics	
Multiple R	0.430687659
R Square	0.18549186
Adjusted R Square	0.156402283
Standard Error	0.069927595
Observations	30

ANOVA

	df	*SS*	*MS*	*F*	*Significance F*
Regression	1	0.031180613	0.031180613	6.376574795	0.017506394
Residual	28	0.136916321	0.004889869		
Total	29	0.168096934			

	Coefficients	*Standard Error*	*t Stat*	*P-value*	*Lower 95%*	*Upper 95%*	*Lower 95.0%*	*Upper 95.0%*
Intercept	-0.261877132	0.138438168	-1.891654131	0.068922277	-0.545454863	0.0217006	-0.545454863	0.0217006
S	0.001367751	0.000541643	2.525188071	0.017506394	0.000258245	0.002477257	0.000258245	0.002477257

Table 18: Regression of Travel Rate F with Regard to Bead Thickness

SUMMARY OUTPUT

Regression Statistics	
Multiple R	0.003373066
R Square	1.13776E-05
Adjusted R Square	-0.035702502
Standard Error	0.07748157
Observations	30

ANOVA

	df	*SS*	*MS*	*F*	*Significance F*
Regression	1	1.91254E-06	1.91254E-06	0.000318576	0.985886142
Residual	28	0.168095022	0.006003394		
Total	29	0.168096934			

	Coefficients	*Standard Error*	*t Stat*	*P-value*	*Lower 95%*	*Upper 95%*	*Lower 95.0%*	*Upper 95.0%*
Intercept	0.085063405	0.066081943	1.287241278	0.208549703	-0.050299319	0.220426129	-0.050299319	0.220426129
F	2.24442E-06	0.000125747	0.017848691	0.985886142	-0.000255336	0.000259825	-0.000255336	0.000259825

As stated, the values that can indicate correlation and significance between the independent and dependent variables are *R*, Significance *F* and the *P*-value. With *R*, the desired value for significance is as close to 1 as possible. For Significance *F* and the *P*-value, the desired value is

small, as these two are linked. Significance *F* should be smaller than the Test *F* value, and the *P*-value should be less than the α value for significance, typically around 0.05.

It is apparent from these regressions that in most cases there was no clear correlation. The one exception to this appeared to be between feed rate *S* and bead thickness. This was the strongest correlation seen between an individual independent and dependent variable. Other variables exemplified some linkage, such as argon flow to x and y error, but it did not provide strong enough evidence for correlation. However, there were several factors to consider as to the potential reason behind this. The most likely reason for this was the difficulty to properly isolate each individual variable. Based on observations during the trial runs, it became apparent by the end of the trials that the input variables had some degree of impact on each other. Because of this, it was difficult to properly isolate one without inadvertently affecting others. Furthermore, the dependent variables were difficult to isolate as well. If for example bead thickness was too large or small, it would alter the x and y dimension of the part as well. What was witnessed instead was print quality varying in response to a combination of changes in parameters rather than any individual parameter being changed. This was evidenced as well by the fact that the overall print error displayed a decreasing trend throughout the trials, as demonstrated in Figure 42.

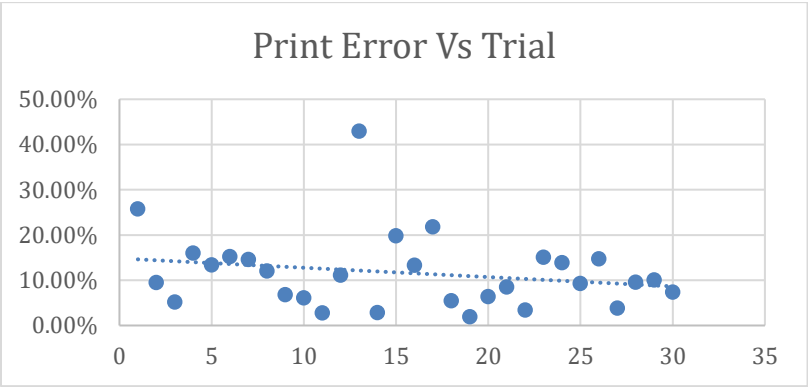

Figure 42: Print Error Vs Trial Number

This indicated that corrections were being made to the print geometry based on the variation of the input parameters. While only one regression of each individual parameter showed clear results, performing regression on the trial number versus the overall error showed that there was a potential correlation between the trial number and the percent error. Table 19 shows the results from a regression of Trial Number with Regard to the Overall Error. As the goal was to reduce error overall with each subsequent test, this shows there was success in this area.

Table 19: Regression of Trial Number with Regard to Overall Error

SUMMARY OUTPUT

Regression Statistics	
Multiple R	0.217703615
R Square	0.047394864
Adjusted R Square	0.013373252
Standard Error	0.082633361
Observations	30

ANOVA

	df	*SS*	*MS*	*F*	*Significance F*
Regression	1	0.009512337	0.009512337	1.393081077	0.247815716
Residual	28	0.191191624	0.006828272		
Total	29	0.20070396			

	Coefficients	*Standard Error*	*t Stat*	*P-value*	*Lower 95%*	*Upper 95%*	*Lower 95.0%*	*Upper 95.0%*
Intercept	0.148216274	0.030943947	4.78983098	4.92667E-05	0.084830473	0.211602076	0.084830473	0.211602076
Trial	-0.002057282	0.001743033	-1.180288557	0.247815716	-0.005627723	0.001513159	-0.005627723	0.001513159

While the *R* value did not provide a strong correlation, there is still evidence for some with it. What is more interesting is the Significance *F* and the *P*-value. The Significance *F* is 0.247, which is lower than the Test *F* value of 1.39. The *P*-value is 0.247 as well, which, while lower than some other tests, is not enough to prove significance. While not conclusive, this is indicative that the overall quality was improving.

Based on this combination of variables, the input values that consistently gave the best results were argon flow set at 25 CFH, feed speed *S* set at 240-250 rpm, and the travel rate *F* set at 500 mm/min. While these input values provided the most consistently successful and accurate prints, more testing would be needed to determine if there is a strong correlation between this. Further, it would be beneficial to develop an understanding of the relationships between input parameters for future work.

The hardness tests yielded interesting results as well. The hardness values recorded was demonstrated to be reasonably repeatable across a range of 21.5 HRB with an average hardness of 78.4 HRB. The standard deviation of this data would be valuable to better understand the amount of variance present.

$$\sigma = \sqrt{\frac{\Sigma(x_i - \mu)^2}{N}} \tag{16}$$

where x_i is the value for each point, μ is the population mean, and N is the number of samples. This value was calculated using Excel, and found to be

$$\sigma = 7.35\ HRB$$

This value seemed slightly higher than desirable for consistent hardness testing; however, upon inspection of the data, a potential reason for this was discovered. On each sample, the first of the three tests was always the lowest, with the hardness typically increasing with each subsequent test on the same sample. Due to the small size of each test sample, it is likely that cold-working was unable to be avoided in the test piece, leading to work-hardening of the material between tests. In this case, the first test value would be the best representative of the hardness of

the printed materials. The hardness data results from just the first test of each sample were taken and compiled in Table 20.

Table 20: First Hardness Test per Sample

Sample Number:	Test Number:	Hardness (HRB):
1	1	67.9
2	1	71.2
3	1	73.4
4	1	69.8
5	1	69.4

By analyzing this smaller subset and removing the error of cold-working, the print hardness was demonstrated to be far more consistent.

$$\bar{H} = \frac{67.9 + 71.2 + \cdots + 69.4}{5}$$

$$R = 73.4 - 67.9$$

$$\bar{H} = 70.3 \text{ HRB}$$

$$R = 5.5\ HRB$$

With this in mind, the adjusted range of hardness became 5.5 HRB and the average hardness became 70.3 HRB. This indicates the process has reasonable consistency in these preliminary tests, though more data would be desirable.

$$\sigma = 1.85\ HRB$$

The new data set provided a much lower standard deviation at 1.85 HRB as opposed to 7.35 HRB. This demonstrates far lower variance in the consistency of material hardness in parts

produced by this method. From this, it can be determined that there is a degree of consistency to this method.

VIII: Conclusion and Future Work

The process of additive manufacturing developed in this research is highly experimental. Little prior work directly comparable to this method was available, and the scope of the project entailed many sub-sections requiring a great deal of analysis, design, implementation, and testing. Due to this, it was difficult to adequately cover all aspects of this design and topic within the timeframe and scope of a Master's Thesis. Despite this, from the observations of this research, the initial results show promise in the viability of this method of additive manufacturing. The results produced by this technology showed consistent production based on the hardness results, and the machine was able to repeatedly produce the desired geometry with good accuracy.

While this lays the groundwork for potential expansion of this technology, much more work is needed to fully develop its capabilities. As mentioned, the relationship between the different independent variables was difficult to determine at this stage. The relationship between these variables could be better characterized through further analysis and testing. This in turn could lead to optimization of this machine. Specifically, a method for fully isolating and testing each variable independently while examining changes to determine significance would be useful. However, it is possible these variables cannot be adequately isolated, as was evidenced by the connections seen in this research. If this is the case, rather than focus on isolating the variables, a method for modeling the relationships between the variables would need to be developed. Utilizing this model, it could be determined what the impact combinations of variables have on the ultimate print quality. A multivariate analysis could be beneficial as well to in order to examine and evaluate all of the inputs in this system simultaneously. This could lead to stronger evidence of particular correlations and provide a better understand of control for this method.

Another area of interest would be to further characterize the material properties of the parts produced further. The hardness data produced by this test validates the consistency of the parts produced by this method, however, yield strength and other characteristics would be necessary when looking at implementing parts produced by this method. Many methods for obtaining material strength are available, such as proposed theoretical models between hardness and strength, tensile testing, and other forms of destructive testing. Material properties data would be the most valuable data after a better understanding of the relationship between parameters.

Several new design considerations could be made as well in further exploration of this technology and its capabilities. For example, potential new designs for the print head optimization could be performed in order to maximize the efficiency of power transfer. The print head created in this research was designed and fabricated based on the ability to perform the desired goal and successfully print material. No major work was done to improve the efficiency and maximize its capabilities. This would be beneficial for future work.

Likewise, the print bead was not optimized theoretically, only experimentally based on the results witnessed during early testing. Multiple forms of optimization could be performed in this area. First, the heat transfer of the bed, specifically into the material being deposited for the build. Secondly, the optimization of surface area for the mesh would be beneficial to examine. Quick experimental examination of this was performed as part of this research, but further work could be done to optimize it. These two factors are likely linked, so the relationship between the two could be explored as well.

There are numerous design areas where modifications could be made and tested. Over the course of this research, multiple iterations of parts and systems were designed, tested, and either implemented, scrapped, or modified. Similarly, there are still several untested options for systems

involved in this research, such as argon delivery to the print head, feed system modifications, motion of the gantry, control software optimization, and many more. Each of these are areas that could require further research and development in order to better improve the application of this technology.

While there is still plenty of opportunity for work to be done on this topic, this project sought to establish the initial concept, design, and prototype of this technology. Though some shortcomings were observed in the first efforts due to the magnitude of the project, promising results were seen. From here, further efforts could one day finalize the design and lead to commercialization and implementation of this as an affordable alternative for metal additive manufacturing.

IX: References

1. Frazier, W.E., *Metal Additive Manufacturing: A Review.* Journal of Materials Engineering and Performance, 2014. **23**(6): p. 1917-1928.
2. Wong, K.V. and A. Hernandez, *A Review of Additive Manufacturing.* ISRN Mechanical Engineering, 2012. **2012**: p. 1-10.
3. Hunko, W.S., *Cold Metal Transfer-Gas Metal Arc Welding (CMT-GMAW) Wire + Arc Additive Manufacturing (WAAM) Process Control Implementation* 2018: p. 520.
4. King, W.E., et al., *Laser powder bed fusion additive manufacturing of metals; physics, computational, and materials challenges.* Applied Physics Reviews, 2015. **2**(4).
5. Seifi, M., et al., *Overview of Materials Qualification Needs for Metal Additive Manufacturing.* Jom, 2016. **68**(3): p. 747-764.
6. Williams, S.W., et al., *Wire + Arc Additive Manufacturing.* Materials Science and Technology, 2016. **32**(7): p. 641-647.
7. Gades, J.S., *Parametric Development of Wire 3D Printing* 2015: p. 150.
8. Song, Y.-A., S. Park, and S.-W. Chae, *3D welding and milling: part II—optimization of the 3D welding process using an experimental design approach.* International Journal of Machine Tools and Manufacture, 2005. **45**(9): p. 1063-1069.
9. Clark, D., M.R. Bache, and M.T. Whittaker, *Shaped metal deposition of a nickel alloy for aero engine applications.* Journal of Materials Processing Technology, 2008. **203**(1-3): p. 439-448.
10. Zinn, S., et al., *Elements of induction heating : design, control, and applications*. 1988, Metals Park, Ohio: ASM International. xv, 335 p.
11. Rudnev, V., D. Loveless, and R. Cook, *Handbook of Induction Heating, 2nd Edition*. 2017.
12. Kaehler, H.W., *Casting Kaiser Aluminum*. 1965, Kaiser Center Oakland, California 94604: Kaiser Aluminum & Chemical Sales. 596.
13. Ammen, C.W., *Metalcasting*. 2000, New York, NY: McGraw-Hill. 434.
14. Chastain, S.D., *Metal Casting: A Sand Casting Manual For the Small Foundry*. First ed. Vol. 1. 2004, Jacksonville, FL. 208.
15. Campbell, J., *Castings*. Second Edition ed. 2003, Oxford: Butterworth-Heinemann. 335.
16. Prasad, V.V., *Preparation of Aluminum Alloy Speciment by Semi-Solid Casting.* National Conference on Emerging Trends in Mechanical Engineering, 2012: p. 3.
17. Midson, S., *A Comparison of Thixocasting and Rheocasting.* World Foundry Congress: p. 10.
18. Salleh, M.S., et al., *An Overview of Semisolid Processing of Aluminium Alloys.* ISRN Materials Science, 2013. **2013**: p. 1-9.
19. Adedayo, A.V., *Development Processes of Globular Microstructure.* Journal of Minerals and Materials Characterization and Engineering, 2011. **10**(7).
20. Pola, A., M. Tocci, and P. Kapranos, *Microstructure and Properties of Semi-Solid Aluminum Alloys: A Literature Review.* Metals, 2018. **8**(3).
21. Midson, S., *Industrial Applications for Aluminum Semi-Solid Castings.* Solid State Phenomena, 2014. **217-218**: p. 487-495.

22. Jackson, A.P., G.R. Wallace, and S. Midson, *Semi-Solid Casting of Aluminum Turbocharger Impellers.* Advanced Materials and Processes, 2010.
23. Saha, P., *Aluminum Extrusion Technology*. 2000, Materials Park, OH: ASM International. 270.
24. Company, R.M., *Designing with Aluminum Extrusions*. 1949, Louisvill, KY: Reynolds Metal Company. 137.
25. Rattanochaikul, T., et al., *Development of aluminum rheo-extrusion process using semi-solid slurry at low solid fraction.* Transactions of Nonferrous Metals Society of China, 2010. **20**(9): p. 1763-1768.
26. Fan, J.S., *Semi-solid Processing of Engineering Alloys by a Twin-Screw Rheomoulding Process.* Materials Science and Engineering, 2000(A299): p. 210-217.
27. **Rice, C.S.**, *Semi-Solid Metal Freeform Fabrication*. 2000, US Department of Energy: Cambridge, MA.
28. Jabbari, A. and K. Abrinia, *Developing thixo-extrusion process for additive manufacturing of metals in semi-solid state.* Journal of Manufacturing Processes, 2018. **35**: p. 664-671.
29. Anzalone, G.C., et al., *A Low-Cost Open-Source Metal 3-D Printer.* IEEE Access, 2013. **1**: p. 803-810.
30. NIST, *Mechanical Properties Testing for Metal Parts Made via Additive Manufacturing: A Review of the State of the Art of Mechanical Property Testing.* National Institute of Standards and Technology, 2012.
31. International, A., *Standard Test Methods for Tension Testing of Metallic Materials.* ASTM E8, 2009.
32. Akhyar, H., *Cooling Rate, Hardness, and Microstructure of Aluminum Cast Alloys.* Materials Science: Materials Review. **1**(1).
33. ASTM International., *Standard Specification for Aluminum Alloys in Ingot and Molten Forms for Castings from All Casting Processes.* ASTM B179-18, 2018.
34. ASTM International., *Standard Test Methods for Rockwell Hardness of Metallic Materials.* ASTM E18-20, 2020

Appendix A: Pictures of Finalized Printer Components

Pre-Purchased Tungsten Nozzle

Stainless Steel Crucible

Carbon Steel Jacket For Stainless Steel Crucible

Updated Ceramic Guide Tube

Ceramic Guide Tube Insert

Fully Assembled Crucible/Nozzle Redesign

Fully Assembled Crucible/Nozzle and Feed Guide

Appendix B: Full Data Set for Geometrical Accuracy Tests

							X dimeinsion theoretical (in)	Avg % Error (X)	Y dimenson theoretical (in)	Avg % Error (Y)	Target Bead Thick	Average Bead Error	
							0.6321	4.43%	1.2221	1.78%	0.0443	9%	
Trial	Argon	tank pres	S	F	Bed Temp Set	Print head set	x dimension (in)	% Error (X)	y dimension (in)	% Error (Y)	Bead Thickness (in)	Bead Thickness Error	Overall Erro
1	23	500	300	750	900	1100	0.631	0.17%	1.25	1.07%	0.034	23.3%	25.76525%
2	23	425	300	750	950	1100	0.638	0.93%	1.209	0.91%	0.041	7.5%	9.52412%
3	23	400	300	750	950	1100	0.624	1.28%	1.211	1.40%	0.043	3.0%	5.19723%
4	23	400	300	500	950	1100	0.63	0.33%	1.205	2.63%	0.038	14.3%	16.01717%
5	23	350	275	600	950	1100	0.626	0.97%	1.19	2.22%	0.04	9.8%	13.36610%
6	25	2250	250	700	800	1200	0.626	0.97%	1.195	3.85%	0.039	12.0%	15.21261%
7	25	2250	250	700	800	1200	0.626	0.97%	1.175	3.28%	0.04	9.8%	14.59350%
8	25	2250	250	600	800	1200	0.624	1.28%	1.182	3.12%	0.041	7.5%	12.08148%
9	25	2250	250	500	800	1200	0.646	2.20%	1.184	1.73%	0.045	1.5%	6.82036%
10	25	2250	250	500	800	1200	0.636	0.62%	1.201	1.56%	0.046	3.8%	6.10293%
11	25	2250	250	500	800	1200	0.635	0.46%	1.203	2.22%	0.044	0.8%	2.77355%
12	25	2225	250	400	800	1200	0.655	3.62%	1.195	2.36%	0.042	5.3%	11.10350%
13	25	2200	300	400	800	1200	0.651	2.99%	1.251	0.91%	0.061	37.6%	42.94880%
14	25	2200	225	400	800	1200	0.635	0.46%	1.211	6.72%	0.045	1.5%	2.87082%
15	25	2200	225	300	800	1200	0.63	0.33%	1.14	1.15%	0.05	12.8%	19.83213%
16	25	2100	200	400	800	1200	0.633	0.14%	1.208	0.65%	0.039	12.0%	13.32621%
17	25	2050	250	500	800	1200	0.685	8.37%	1.23	0.83%	0.05	12.8%	21.79731%
18	25	2050	250	500	800	1200	0.652	3.15%	1.212	0.83%	0.045	1.5%	5.47844%
19	25	2050	240	500	800	1200	0.63	0.33%	1.212	0.83%	0.044	0.8%	1.91055%
20	22	2050	240	500	800	1200	0.63	0.33%	1.212	1.46%	0.042	5.3%	6.42183%
21	32	1750	240	500	800	1200	0.621	1.76%	1.24	1.48%	0.042	5.3%	8.48390%
22	23	1450	240	500	800	1200	0.635	0.46%	1.204	1.07%	0.045	1.5%	3.44360%
23	22	1450	250	450	800	1200	0.64	1.25%	1.209	0.91%	0.05	12.8%	15.10368%
24	23	1450	250	500	800	1200	0.631	0.17%	1.211	0.56%	0.05	12.8%	13.86425%
25	23	1450	250	450	800	1200	0.635	0.46%	1.229	1.81%	0.048	8.3%	9.29407%
26	22	1450	250	450	800	1200	0.633	0.14%	1.2	1.24%	0.05	12.8%	14.73270%
27	22	1450	250	450	800	1200	0.639	1.09%	1.207	1.32%	0.045	1.5%	3.83094%
28	25	1450	250	450	800	1200	0.632	0.02%	1.206	0.99%	0.048	8.3%	9.60390%
29	25	1450	250	450	800	1200	0.622	1.60%	1.21	1.97%	0.041	7.5%	10.10674%
30	25	1450	250	450	800	1200	0.633	0.14%	1.198	100.00%	0.042	5.3%	7.37756%

Appendix C: Equipment Used

Fabrication of Parts for Machine:

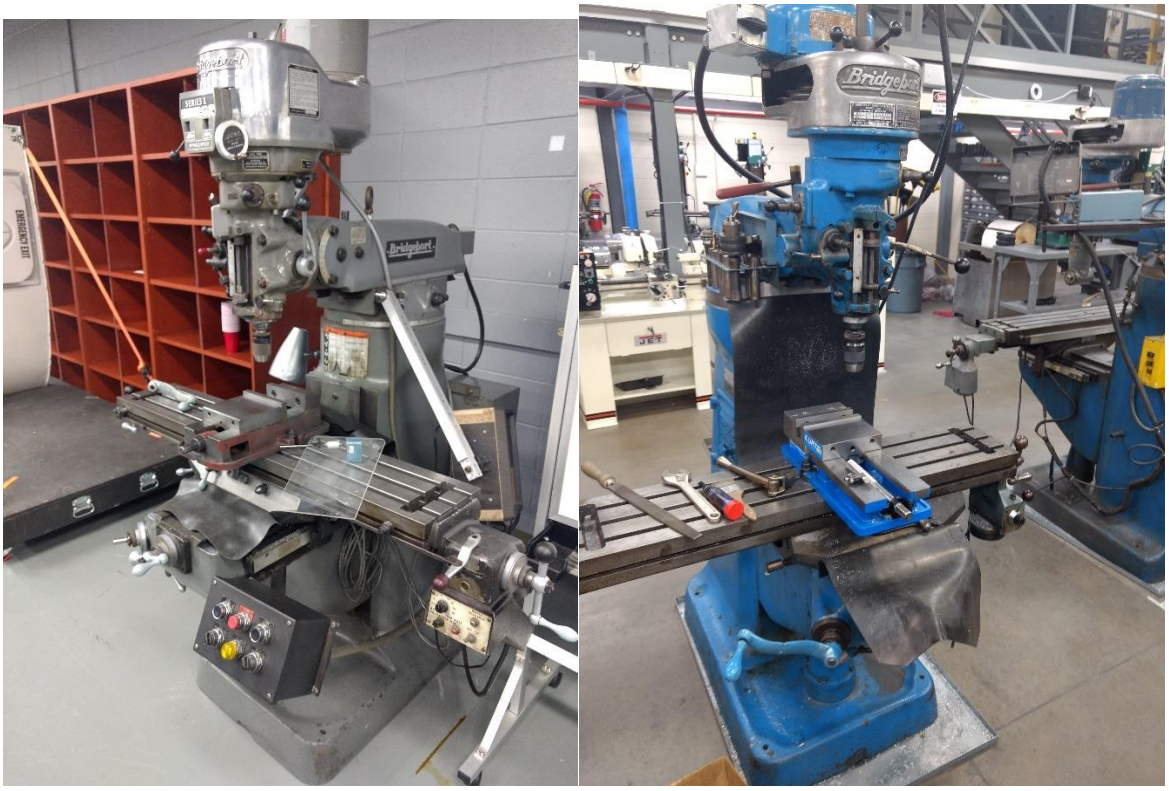

Bridgeport Series I Vertical End MillS

Wellsaw Horizontal Band Saw

DoAll Vertical Band Saw

Cincinnati Arrow CNC Mill

South Bend 450 Lathe

Monarch 10EE Lathe

Sample Preparation:

Struers LaboPress-3 Hot Mount Machine

Buehler Rotary Surface Grinder

Buehler Stationary Surface Sander

Sample Evaluation:

Denver Instrument Gram Scale

Wilson Silver Series Rockwell Hardness Tester

Appendix D: Thermal Study in SolidWorks

Model

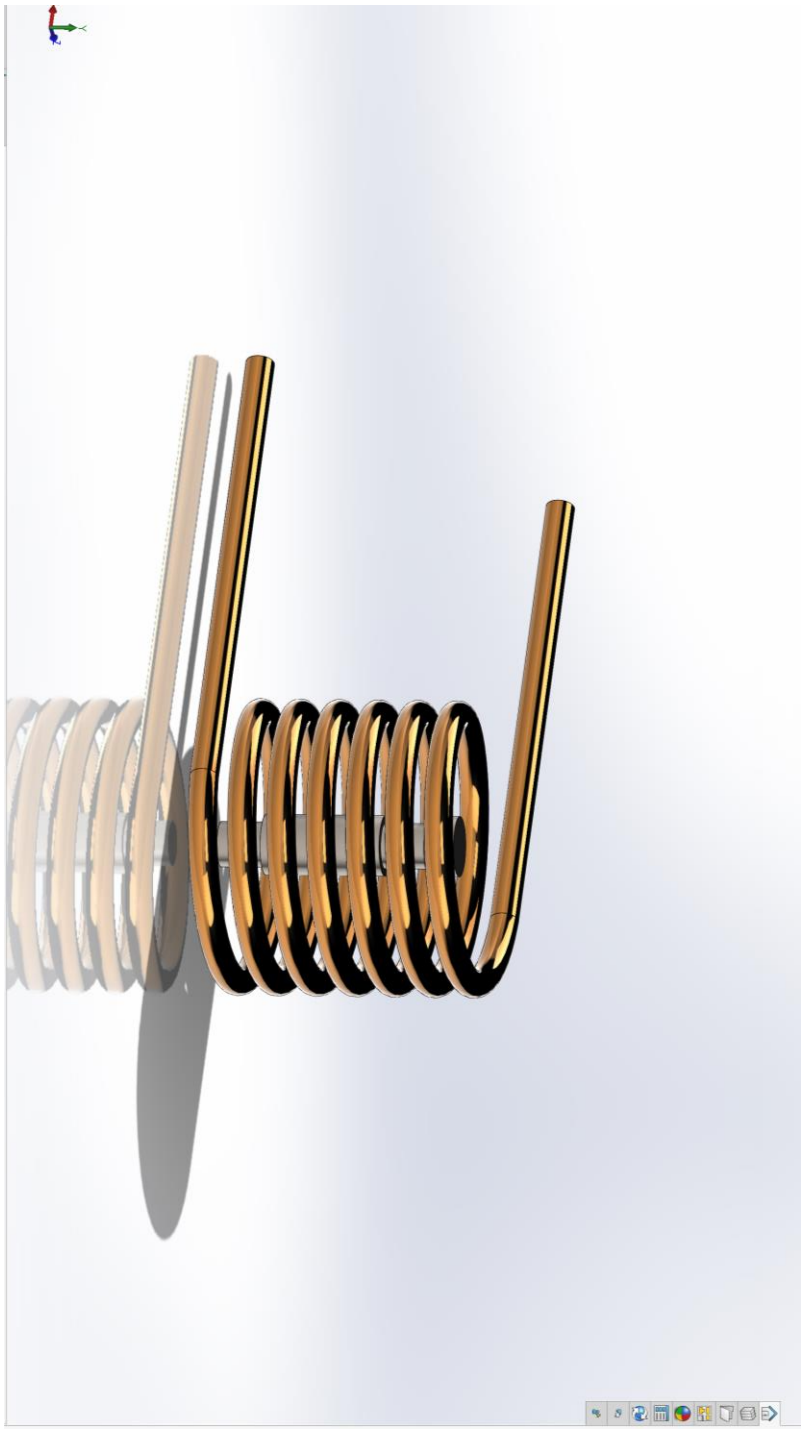

Results:

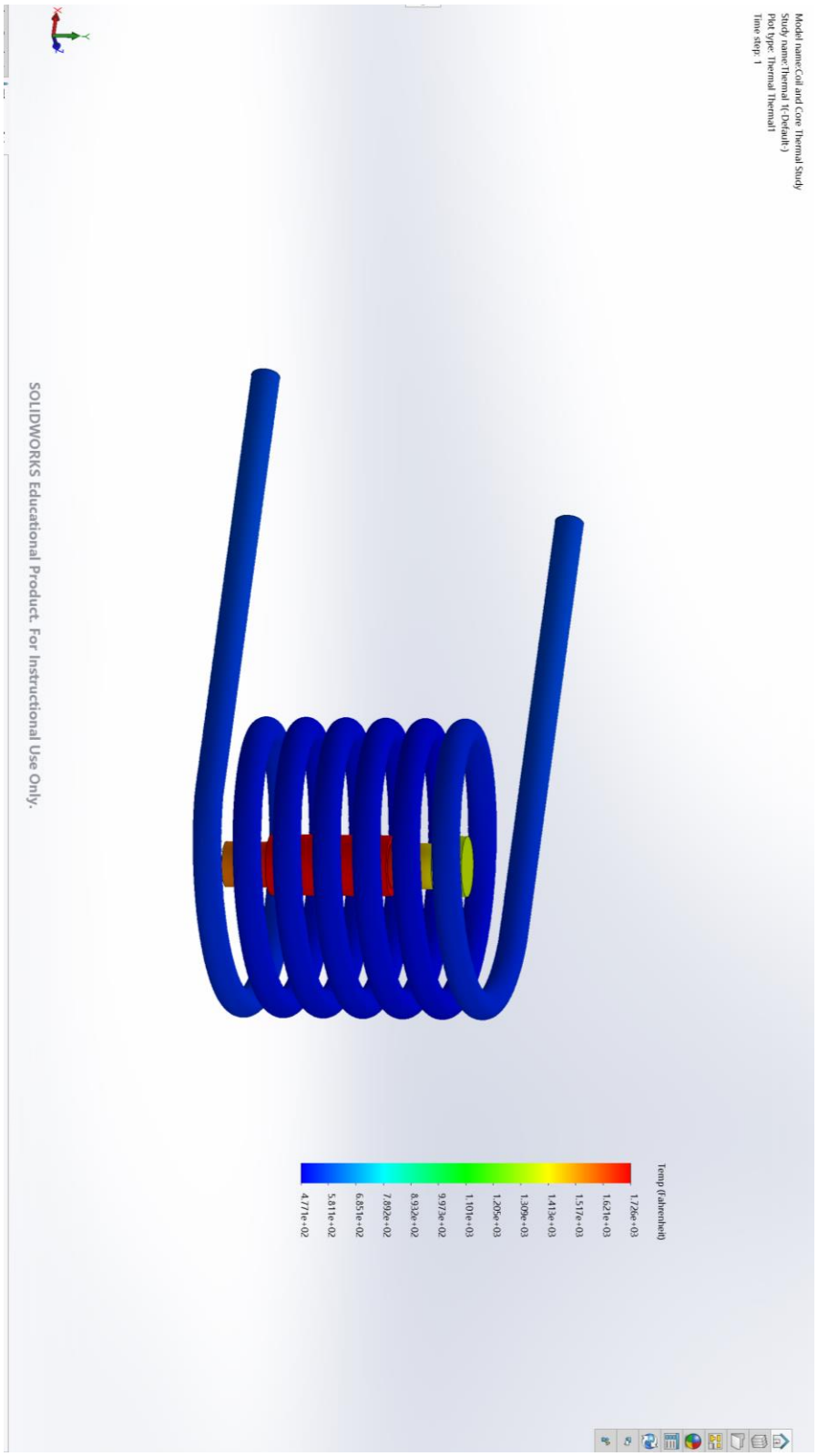
Model name:Coil and Core Thermal Study
Study name:Thermal 1(-Default-)
Plot type: Thermal Thermal1
Time step: 1
SOLIDWORKS Educational Product. For Instructional Use Only.
Temp (Fahrenheit)
1.726e+03
1.621e+03
1.517e+03
1.413e+03
1.309e+03
1.205e+03
1.101e+03
9.973e+02
8.932e+02
7.892e+02
6.851e+02
5.811e+02
4.771e+02